Direct Position Determination in Asynchronous Sensor Networks

Fuhe Ma, Zhang-Meng Liu, and Fucheng Guo

***Abstract*—Source positioning using time difference of arrival (TDOA) has received much research interest in the field of vehicular technology during the past decades. In practice, sensor networks may be disturbed by clock biases, and extra active anchor sources with known positions could be exploited to calibrate these clock biases. Although there exist numerous two-step localization methods on this issue, they are inherently suboptimal. In this paper, we address the TDOA-based source direct position determination (DPD) problem in asynchronous sensor networks. First, the clock biases are demonstrated via theoretical analyses to cast significant influences on localization accuracy negatively. Then, a DPD method is proposed, exploiting anchor sources to jointly calibrate clock biases and determine the unknown source position, which integrates an expectation-maximization (EM) algorithm and a Gauss–Newton algorithm for coarse and refined parameter estimation, respectively. In this way, the computational load of the considered DPD problem is reduced considerably compared with exhaustive search-based DPD method. Moreover, the Cramér–Rao lower bound is derived for the considered DPD problem, and how anchor sources affect the localization performance is further analyzed. Simulation results demonstrate the necessity of clock bias calibration and the satisfactory performance of the proposed method.**

***Index Terms*—Direct position determination (DPD), time difference of arrival (TDOA), clock bias, anchor source, asynchronous sensor network, expectation maximization (EM).**

I. Introduction

PASSIVE localization has been a classic topic during the past decades. It is widely applied to numerous applications in the field of vehicular technology, such as vehicle emergency rescue, automatic driving, traffic management and navigation, etc [1]–[4].

To localize the source, multiple spatially separated sensors are deployed to collect the signals emitted from the source. Conventionally, this source positioning procedure is carried out within two steps, and the associated localization methods are termed two-step methods. In the first step, the intermediate parameters are estimated, such as received signal strength (RSS) [2], [5], direction of arrival (DOA) [6], time of arrival (TOA) [5], [7], time difference of arrival (TDOA) [3] and frequency difference of arrival (FDOA) [8], [9]. Then these intermediate parameters are exploited to determine the source position during the second step. Among existing source localization methods, TDOA-based two-step methods are widely researched [3], [4], [10], [11], and many maximum-likelihood (ML) solvers have been proposed in synchronized sensor networks. Particularly, closed-form two-step methods for TDOA-based source positioning are very popular [3], [4], [11], [12]. They are usually computationally efficient and able to achieve the Cramér Rao lower bound (CRLB) under mild Gaussian measurement error conditions.

In two-step localization methods, the intermediate parameters are estimated independently during the first step, without considering the constraint that all the intermediate parameters are correlated to each other according to the unknown source position [13], [14]. As a result, two-step methods are inherently suboptimal, and their performance degrades significantly under large noise conditions. Recently, the direct position determination (DPD) methods, which are also termed one-step localization, have become very popular in the signal processing community [14]–[20]. Different from two-step localization methods, the intermediate parameters (e.g., DOA, TDOA, FDOA) are not estimated in DPD methods, and the one-step cost function is constructed via projecting directly the received signals into the source position space. By searching and selecting the position candidate that maximizes the cost function, the source position estimate is obtained and the correlation between different intermediate parameters is inherently taken into consideration. In this way, DPD methods generally obtain improved localization accuracy and enhanced adaptability to low signal to noise ratios (SNRs) compared to the two-step methods [14]–[17]. However, as the DPD cost functions do not lend themselves to closed form solutions, exhaustive search in high-dimensional source position space is usually resorted to, which is computationally more expensive than the two-step methods.

In this paper, the TDOA-based source localization problem is considered, where multiple sensors are assumed to work with independent clocks. For the sake of reducing equipment complexity, there is no dedicated hardware available, such as GPS receivers or atom clocks on each sensor, to guarantee time synchronization, thus introducing clock biases. The above mentioned TDOA-based two-step and DPD localization algorithms [3], [4], [11], [12], [16] are developed under the assumption that the sensors are perfectly synchronized. Their localization performance degrades significantly in asynchronous sensor networks, and thus clock biases should be calibrated when TDOAs are used

Manuscript received February 27, 2019; revised June 3, 2019; accepted July 7, 2019. Date of publication July 15, 2019; date of current version September 17, 2019. This work was partially supported by the National Natural Science Foundation of China under Grant 61771477. The review of this paper was coordinated by Prof. A. Jamalipour. *(Corresponding author: Fuhe Ma.)*

The authors are with the State Key Laboratory of Complex Electromagnetic Environment Effects on Electronics and Information System (CEMEE), National University of Defense Technology, Changsha 410073, China (e-mail: mafuhe14@nudt.edu.cn; liuzhangmeng@nudt.edu.cn; gfcly75@163.com).

Digital Object Identifier 10.1109/TVT.2019.2928638

for source localization. When only a single source is present in the asynchronous sensor networks, the number of unknown parameters, i.e., all the clock biases and source position, is larger than the number of independent TDOA measurements. This leads to non-unique solutions, as could be revealed in Section VI via analyzing the derived CRLB. To calibrate the unknown clock biases, extra active anchor sources with known positions, e.g., broadcasting stations or active sensors, should be exploited.

Numerous works have been proposed recently [21]–[29] to cope with joint clock bias calibration and source localization in asynchronous sensor networks. In [21], two preprocessing techniques were presented to remove the effects of unknown clock biases using pseudo TOA measurements. In [22]–[24], multiple source positions were estimated jointly in the presence of sensor synchronization errors, via the weighted least squares (WLS) method, expectation maximization (EM) algorithm or Lagrange programming neural network (LPNN) method. In [25], [26], the clock biases were estimated using the convex optimization techniques. Particularly, clock bias calibration using anchor sources with known positions is ubiquitous and there exist many works focused on it. In [27]–[30], the offsets (and skews) of clock biases were estimated with the aid of anchor source signals, and the source positions were estimated using calibrated measurements. In these works the sensors acted as both receivers and active anchor sources, thus synchronization was realized through least squares (LS) techniques. The above mentioned algorithms localize the source in two-steps by measuring some intermediate parameters (TOAs or TDOAs). Although these two-step methods perform well under high SNR conditions, they are intrinsically suboptimal compared to the one step DPD methods. Unfortunately, there exists no DPD algorithm for source positioning in asynchronous sensor networks. Moreover, the associated CRLB derivation and performance analysis are not available.

With this regards, we address the source DPD problem in asynchronous sensor networks with the aid of multiple anchor sources with known positions. Theoretical error analysis is conducted to prove that uncalibrated clock bias would deteriorate the source positioning accuracy of conventional DPD algorithms. Then a DPD cost function is developed to jointly calibrate the clock biases and localize the source. Instead of applying the computationally prohibitive exhaustive search to solve the developed cost function, we derive an EM-based DPD method to obtain coarse estimates of the source position and clock biases, which are then refined jointly via Gauss-Newton (GN) iterations. The overall computational load is thus largely reduced as both procedures involve only computationally cheap numerical calculations compared with the high-dimensional exhaustive search. The CRLB for the problem considered is then derived to evaluate the performance of the proposed method. Deep insights are further provided based on the CRLB to show how anchor sources affect the localization performance. These theoretical analyses and the performance of the proposed method are validated via simulation results.

The contributions of this paper mainly include:

- A DPD cost function is formulated using multiple anchor sources to localize the source of interest in asynchronous sensor networks, which differs inherently from its two-step counterparts.
- The CRLB for source DPD with the aid of anchor sources in asynchronous sensor networks is derived.
- A DPD method, which is composed of an EM-based coarse estimation procedure and a GN iteration procedure, is developed to solve the joint synchronization and localization problem. The proposed method reduces the computational load tremendously compared with exhaustive search.
- Theoretical analyses are carried out to reveal the effects of non-calibrated clock biases and anchor sources on localization performance.

TABLE I
IMPORTANT NOTATIONS

$\boldsymbol{A}^T$, $\boldsymbol{A}^H$: The transpose and Hermitian transpose of matrix $\boldsymbol{A}$.
$\boldsymbol{A}^{-1}$: The inverse of matrix $\boldsymbol{A}$.
Re$\{\boldsymbol{A}\}$, Im$\{\boldsymbol{A}\}$: The real and imaginary parts of matrix $\boldsymbol{A}$.
Diag$(\boldsymbol{a})$: The diagonal matrix with diagonal entries given by $\boldsymbol{a}$.
blkdiag$(\boldsymbol{A}, \boldsymbol{B})$: The block diagonal matrix formed by $\boldsymbol{A}$ and $\boldsymbol{B}$.
$\hat{\boldsymbol{A}}$: The estimate of $\boldsymbol{A}$.
$\|\cdot\|$: The Euclidean distance operator in Cartesian coordinate system.
$E\{\cdot\}$: The statistical expectation operator.
$\lceil\cdot\rceil$: The ceiling operator.
$\mathbf{1}$ and $\mathbf{0}$: The all-ones vector and zero vector.
$\mathbf{I}_n$: The identity matrix of size n.
$\mathbf{O}_{m\times n}$: Zero matrix with m rows and n columns.
$\boldsymbol{u}_0$: The coordinates of the source of interest.
$\boldsymbol{u}$: An arbitrarily assumed source position variable.
$\boldsymbol{u}_i, i>0$: The coordinates of the ith sensor.
$\boldsymbol{u}_k^{(c)}$: The coordinates of the kth anchor source.
$\boldsymbol{r}_i$: Source signal vector received at the ith sensor.
$\boldsymbol{r}_i^k$: Signal vector from anchor source k received at the ith sensor.
$\bar{\boldsymbol{r}}_i$ and $\bar{\boldsymbol{r}}_i^k$: Noise-free versions of $\boldsymbol{r}_i$ and $\boldsymbol{r}_i^k$.
$\boldsymbol{\alpha}=[\alpha_{2,1},\cdots,\alpha_{M,1}]^T$: Source signal relative amplitude vector.
$\boldsymbol{\alpha}^{(c)}=[\alpha_{2,1}^{(c)},\cdots,\alpha_{M,1}^{(c)}]^T$: Anchor source signal relative amplitude.
δ_i: The clock bias between sensor $i+1$ and sensor 1.
$\boldsymbol{F}$: The fast Fourier transform matrix.

The rest of the paper is organized as follows. Section II formulates the TDOA-based (or time delay-based) DPD problem using multiple anchor sources in asynchronous sensor networks. Section III analyzes the influences of clock biases on DPD accuracy if they are not calibrated. Section IV develops the proposed DPD method for joint source positioning and clock bias calibration. Section V derives the CRLB for the considered DPD problem. Section VI provides insights into the influences of anchor sources on localization performance of the proposed method. Section VII presents the simulation results and the relevant discussions. Section VIII offers concluding remarks. For notational simplicity, a list of important notations is provided in Table I.

II. PROBLEM FORMULATION

Denote the dimension of the localization scenario as d. For illustration purpose, a two-dimensional (2D) localization scenario $(d=2)$ is considered in this paper, which can be readily

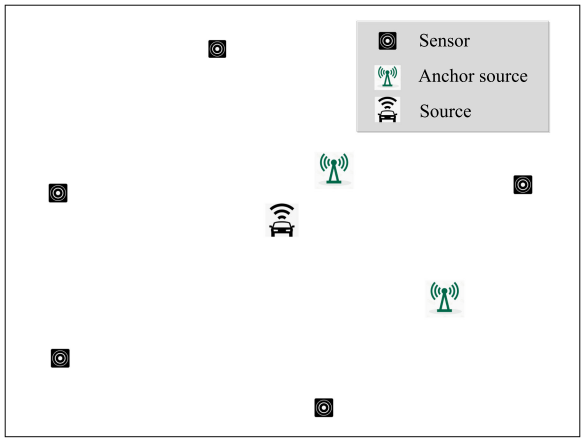

Fig. 1. Schematic diagram for the considered localization scenario. Five sensors are used here for simplicity. Two broadcast stations serve as anchor sources and the source to be localized is the vehicle-mounted emitter.

extended to three-dimensional (3D) case by setting $d = 3$ and expanding the 2D coordinates into 3D. The source emits uncooperative signals at the unknown location $\boldsymbol{u}_0 = [x, y]^T$. A total of M spatially separated sensors are deployed to passively collect signals transmitted from the source $\boldsymbol{u}_0$, and the position of the ith sensor is denoted by $\boldsymbol{u}_i = [x_i, y_i]^T$ for $i = 1, 2, \ldots, M$, which is assumed to be precisely known. As there are no GPS devices or atom clocks available for time synchronization, clock biases are present and sensors are asynchronous. To calibrate these clock biases, K_c anchor sources that transmit uncooperative signals from known positions $\boldsymbol{u}_k^{(c)} = [x_k^c, y_k^c]^T, k = 1, 2, \ldots, K_c$, are further exploited. Without loss of generality, we assume that the signals arrive at the sensors along the line of sight (LOS) path, which is practical in outdoor applications. Receiving the signals from both the source $\boldsymbol{u}_0$ and anchor sources $\boldsymbol{u}_k^{(c)}$ and transmitting these signals to a central processing station via wireless communication, the source position $\boldsymbol{u}_0$ could be determined in a DPD framework. A schematic diagram for the considered scenario is given in Fig. 1, where we would like to localize the vehicle-mounted source with the aid of multiple sensors and anchor sources (broadcasting stations).

At the unknown time instant t_0, the source radiates a signal $s(t - t_0)$, and its received replica at the ith sensor is given by

$$r_i(t) = \alpha_i s(t - t_0 - \|\boldsymbol{u}_0 - \boldsymbol{u}_i\|/c - \tau_i) + w_i(t), \quad (1)$$

where α_i is the signal attenuation factor, τ_i is the bias between the local clock time of the ith sensor and the reference clock due to sensor network asynchronization, c denotes the signal propagation speed, and $w_i(t)$ is the additive white Gaussian noise at the ith sensor with mean zero and variance σ_n^2. The noises are assumed to be uncorrelated with the signals, and $E\{w_i(t)w_q(t)\} = 0$ for $i \neq q$. Meanwhile, the transmitted signal from anchor source k, i.e., $s_k^{(c)}(t - t_k)$, is received at the ith sensor, which is given as

$$r_i^k(t) = \alpha_i^{(c)} s_k^{(c)}(t - t_k - \|\boldsymbol{u}_k^{(c)} - \boldsymbol{u}_i\|/c - \tau_i) + w_i^k(t), \quad (2)$$

where $\alpha_i^{(c)}$ is the signal amplitude at the ith sensor, t_k is the unknown transmit time instant of the kth anchor source and $w_i^k(t)$ is the additive white Gaussian noise, which is also zero-mean with variance σ_n^2. Generally, clean templates for anchor source signals are not available, because they may be uncooperative.

The signal TDOAs of the unknown source $\boldsymbol{u}_0$ and the kth anchor source $\boldsymbol{u}_k^{(c)}$ between the ith and qth sensors are given, respectively, as

$$\begin{aligned} t_{i,q} &= \frac{1}{c}\big(\|\boldsymbol{u}_0 - \boldsymbol{u}_i\| - \|\boldsymbol{u}_0 - \boldsymbol{u}_q\|\big) + (\tau_i - \tau_q) \\ t_{i,q}^k &= \frac{1}{c}\big(\|\boldsymbol{u}_k^{(c)} - \boldsymbol{u}_i\| - \|\boldsymbol{u}_k^{(c)} - \boldsymbol{u}_q\|\big) + (\tau_i - \tau_q), \end{aligned} \quad (3)$$

where t_0 and t_k have been canceled out during the correlation process, and the unknown subtraction $\tau_i - \tau_q$ is the clock bias between the ith and qth sensors.

By examining (3), one can find that two constraints are inherently considered in our model: 1) all $t_{i,q}, i \neq q$ are correlated according to the source position $\boldsymbol{u}_0$; 2) $t_{i,q}$ and $t_{i,q}^k, k = 1, 2, \ldots, K_c$ are contaminated with the same clock bias $(\tau_i - \tau_q)$. These two constraints are *ignored* by the two-step methods where TDOAs $t_{i,q}$ and $t_{i,q}^k$ are measured independently, which accounts for the suboptimal property of conventional two-step methods.

Note that we only need to determine $M - 1$ independent clock biases (i.e., $\tau_{i+1} - \tau_1$ for $i = 1, \ldots, M - 1$) to calibrate the synchronization error of M sensors. Without loss of generality, we *scale the clock biases by constant c and use* $\delta_i = c(\tau_{i+1} - \tau_1), i = 1, 2, \ldots, M - 1$ *to denote them instead* throughout this paper, and the measuring unit of clock biases is given by 'm', which is short for '*meter*'.

Collect the received signals in discrete form, i.e., $r_i[n] \equiv r_i(n/f_s), n = 1, 2, \ldots, N$ with a sampling rate of f_s, where N is the sample number. According to the property of Fourier transform, one obtains

$$\begin{aligned} \boldsymbol{r}_i &= \bar{\boldsymbol{r}}_i + \boldsymbol{w}_i \\ \bar{\boldsymbol{r}}_i &= \frac{\alpha_i}{\alpha_1} \boldsymbol{F}^H \boldsymbol{\Gamma}_{i,1} \boldsymbol{F} \bar{\boldsymbol{r}}_1, \end{aligned} \quad (4)$$

where $\bar{\boldsymbol{r}}_i$ is the noiseless version of $\boldsymbol{r}_i$, and $\boldsymbol{r}_i = [r_i[1], r_i[2], \ldots, r_i[N]]^T$ is the signal vector at the ith sensor. $\boldsymbol{w}_i = [w_i[1], w_i[2], \ldots, w_i[N]]^T$ is the noise vector, and

$$\begin{aligned} \boldsymbol{\Gamma}_i &= \text{Diag}\left(\exp(j2\pi \boldsymbol{n} f_s/N(\|\boldsymbol{u}_0 - \boldsymbol{u}_i\|/c + \tau_i + t_0))\right) \\ \boldsymbol{\Gamma}_{i,1} &= \boldsymbol{\Gamma}_i^H \boldsymbol{\Gamma}_1. \end{aligned} \quad (5)$$

$\boldsymbol{F} = \exp(-j2\pi \boldsymbol{n}\boldsymbol{n}^T/N)$ is the discrete time Fourier transform (DTFT) matrix, in which $\boldsymbol{n} = [-N/2, -N/2 + 1, \ldots, N/2 - 1]^T$ and j is the imaginary unit. For anchor source signals, we have

$$\begin{aligned} \boldsymbol{r}_i^k &= \bar{\boldsymbol{r}}_i^k + \boldsymbol{w}_i^k \\ \bar{\boldsymbol{r}}_i^k &= \frac{\alpha_i^{(c)}}{\alpha_1^{(c)}} \boldsymbol{F}^H \boldsymbol{\Gamma}_{i,1}^k \boldsymbol{F} \bar{\boldsymbol{r}}_1^k, k = 1, 2, \ldots, K_c, \end{aligned} \quad (6)$$

where $\boldsymbol{w}_i^k = [w_i^k[1], w_i^k[2], \ldots, w_i^k[N]]^T$, $\boldsymbol{r}_i^k = [r_i^k[1], r_i^k[2], \ldots, r_i^k[N]]^T$ and

$$\begin{aligned}\boldsymbol{\Gamma}_i^k &= \mathrm{Diag}\big(\exp(j2\pi \boldsymbol{n} f_s/N(\|\boldsymbol{u}_k^{(c)} - \boldsymbol{u}_i\|/c + \tau_i + t_k))\big)\\ \boldsymbol{\Gamma}_{i,1}^k &= (\boldsymbol{\Gamma}_i^k)^H \boldsymbol{\Gamma}_1^k.\end{aligned} \tag{7}$$

The problem is to jointly estimate the source position $\boldsymbol{u}_0$ and clock bias δ_i using all the collected signals, i.e., $\boldsymbol{r}_i$ and $\boldsymbol{r}_i^k$ for $i = 1, 2, \ldots, M$ and $k = 1, \ldots, K_c$. In the following section, we first analyze the influence of non-zero clock biases on localization accuracy if they are neglected, so as to validate the necessity of clock bias calibration.

III. Influence of Clock Biases on Localization Accuracy

In this section, we conduct error analysis of conventional time delay-based DPD algorithm [16] when the undesirable clock biases are present. As the mean square error (MSE) of source position estimate is nonlinear with respect to (w.r.t.) clock biases, it is rather difficult to precisely evaluate the effect of nonzero δ_i on localization performance. Therefore, the first-order Taylor expansion is utilized to ease the derivation and gain insights. In the problem being addressed in this paper, only the source position is of interest to us, and the relative amplitudes $\alpha_{i,1} = \alpha_i/\alpha_1, i = 2, 3, \ldots, M$ are nuisance parameters. For ease of illustration, $\alpha_{i,1}$ is assumed known during the analysis procedure, but the conclusions still hold when $\alpha_{i,1}$ is unknown. When the clock biases δ_i for $i = 1, 2, \ldots, M-1$ are not calibrated, the pseudo cost function in conventional DPD is given by

$$C_{\text{pseudo}}(\boldsymbol{u}) = -\frac{1}{\sigma_n^2}\sum_{i=1}^{M}\big\{(\boldsymbol{r}_i - \boldsymbol{g}_i(\boldsymbol{u}))^H(\boldsymbol{r}_i - \boldsymbol{g}_i(\boldsymbol{u}))\big\}, \tag{8}$$

where

$$\begin{aligned}\boldsymbol{g}_i(\boldsymbol{u}) &= \alpha_{i,1}\boldsymbol{F}^H\tilde{\boldsymbol{\Gamma}}_{i,1}\boldsymbol{F}\bar{\boldsymbol{r}}_1\\ \tilde{\boldsymbol{\Gamma}}_{i,1} &= \mathrm{Diag}\left(\exp(j2\pi \boldsymbol{n} f_s(\|\boldsymbol{u} - \boldsymbol{u}_1\| - \|\boldsymbol{u} - \boldsymbol{u}_i\|)/(Nc))\right)\end{aligned}$$

overlooks the effect of δ_{i-1}. By definition, we have $\alpha_{1,1} = 1$ and $\tilde{\boldsymbol{\Gamma}}_{1,1} = \boldsymbol{I}_N$.

When clock bias is adequately small, the first-order Taylor expansion [31] is valid within the vicinity of $\boldsymbol{u}_0$. This expansion helps to linearize $\boldsymbol{g}_i(\boldsymbol{u})$ around $\boldsymbol{u}_0$ to yield the following approximation given by

$$\boldsymbol{g}_i(\boldsymbol{u}) \approx \boldsymbol{g}_i(\boldsymbol{u}_0) + \boldsymbol{G}_i(\boldsymbol{u}_0)(\boldsymbol{u} - \boldsymbol{u}_0), \tag{9}$$

where $\boldsymbol{G}_i(\boldsymbol{u}) = \frac{\partial \boldsymbol{g}_i(\boldsymbol{u})}{\partial \boldsymbol{u}}$ is the Jacobian matrix given by

$$\boldsymbol{G}_i(\boldsymbol{u}_0) = \alpha_{i,1}\boldsymbol{F}^H\tilde{\boldsymbol{\Gamma}}_{i,1}(\boldsymbol{u}_0)\tilde{\boldsymbol{n}}\boldsymbol{F}\bar{\boldsymbol{r}}_1(\boldsymbol{\rho_i} - \boldsymbol{\rho_1})^T, \tag{10}$$

where $\boldsymbol{\rho}_i = \frac{\boldsymbol{u}-\boldsymbol{u}_i}{\|\boldsymbol{u}-\boldsymbol{u}_i\|}$ and $\tilde{\boldsymbol{n}} = -j\frac{2\pi f_s}{Nc}\mathrm{Diag}(\boldsymbol{n})$. Substituting the approximation in (9) into the cost function in (8) and minimizing the cost function yield the position estimate

$$\begin{aligned}\hat{\boldsymbol{u}} = \boldsymbol{u}_0 + \mathrm{Re}\Bigg\{&\left(\sum_{i=2}^{M}\boldsymbol{G}_i(\boldsymbol{u}_0)^H\boldsymbol{G}_i(\boldsymbol{u}_0)\right)^{-1}\\ &\times\sum_{i=2}^{M}\boldsymbol{G}_i(\boldsymbol{u}_0)^H(\boldsymbol{r}_i - \boldsymbol{g}_i(\boldsymbol{u}_0))\Bigg\}.\end{aligned} \tag{11}$$

Moreover, taking the first-order Taylor expansion of $\boldsymbol{r}_i$ in (4) w.r.t. δ_{i-1} gives

$$\boldsymbol{r}_i - \boldsymbol{g}_i(\boldsymbol{u}_0) \approx \alpha_{i,1}\boldsymbol{F}^H\tilde{\boldsymbol{\Gamma}}_{i,1}(\boldsymbol{u}_0)\tilde{\boldsymbol{n}}\boldsymbol{F}\bar{\boldsymbol{r}}_1\delta_{i-1} + \boldsymbol{G}_i(\boldsymbol{u}_0)\boldsymbol{\epsilon}, \tag{12}$$

where $\boldsymbol{\epsilon}$ is the equivalent localization error caused by the Gaussian noise $\boldsymbol{w}_i$. Substituting (12) into (11) and after some straightforward mathematical derivations, the estimation error of source position can be obtained by subtracting the true source position $\boldsymbol{u}_0$ from both sides of (11) as

$$\boldsymbol{\Delta u} = \hat{\boldsymbol{u}} - \boldsymbol{u}_0 = \boldsymbol{\zeta} + \boldsymbol{\epsilon}, \tag{13}$$

where

$$\begin{aligned}\boldsymbol{\zeta} = &\left(\sum_{i=2}^{M}\alpha_{i,1}^2(\boldsymbol{\rho}_i - \boldsymbol{\rho}_1)(\boldsymbol{\rho}_i - \boldsymbol{\rho}_1)^T\right)^{-1}\\ &\times\left(\sum_{i=2}^{M}\alpha_{i,1}^2(\boldsymbol{\rho}_i - \boldsymbol{\rho}_1)\delta_{i-1}\right),\end{aligned} \tag{14}$$

which is the error term caused by ignoring the nonzero clock biases in conventional DPD algorithm.

From the expression in (13) one can conclude that $E\{\boldsymbol{\Delta u}\} \neq \boldsymbol{0}$, which indicates that overlooking the clock biases results in localization biases. Moreover, noticing the fact that $\boldsymbol{\zeta}$ is uncorrelated with $\boldsymbol{\epsilon}$, the MSE matrix of conventional DPD in asynchronous sensor networks can be obtained as

$$\mathrm{MSE}(\boldsymbol{u}) = \boldsymbol{\zeta}\boldsymbol{\zeta}^T + E\{\boldsymbol{\epsilon}\boldsymbol{\epsilon}^T\}. \tag{15}$$

On the right hand side of (15), the first term roots in the effects of clock biases, and the second term accounts for the perturbation noise $\boldsymbol{w}_i$. The results in (13) and (15) indicate that, when there are clock biases, simply neglecting them will deteriorate the DPD accuracy. To gain deeper insights, the expression of localization bias in (14) reveals that this localization bias is linearly proportional to δ_i.

It is illustrated via simulation results in Fig. 2 of Section VII that the localization biases are approximately $\|\boldsymbol{\zeta}\| = 12.6$ m for $\delta_i = 20$ m and $\|\boldsymbol{\zeta}\| = 31.5$ m for $\delta_i = 50$ m, respectively, for the given configuration, and these localization biases dominate in the localization root mean squares error (RMSE). Therefore, the clock biases should be calibrated when estimating the source position. Although all the clock biases are set to the same value in generating Fig. 2, it does not affect the generality of the obtained analysis results.

In the next section, we shall propose a DPD method to jointly estimate the source position $\boldsymbol{u}_0$ and calibrate the clock biases $\delta_i, i = 1, 2, \ldots, M-1$ by exploiting signals from source $\boldsymbol{u}_0$ and anchor sources $\boldsymbol{u}_k^{(c)}$.

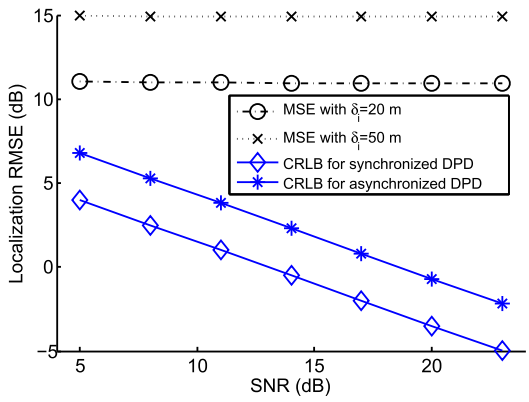

Fig. 2. The negative effects of clock biases. The open diamond denotes the CRLB curve of DPD when no clock biases are present. The star represents the CRLB curve of DPD in the presence of clock biases. The open circle and cross denote the localization RMSEs of conventional DPD method that ignores the clock biases.

IV. Joint Clock Bias Calibration and Source Localization

A. Derivation of the Cost Function

In this subsection, the cost function of the proposed DPD estimator is given. Define the parameter vector as $\boldsymbol{\theta} = [\boldsymbol{\delta}^T, \boldsymbol{u}^T]^T$ with $\boldsymbol{\delta} = [\delta_1, \delta_2, \ldots, \delta_{M-1}]^T$ being the unknown clock bias vector. By using the unknown $\bar{\boldsymbol{r}}_1$ and $\bar{\boldsymbol{r}}_1^k$ as the reference signals, the log likelihood function of received signals is given by

$$\begin{aligned} Q(\boldsymbol{\theta}) = & -\sum_{i=1}^{M} \|\boldsymbol{r}_i - \alpha_{i,1}\boldsymbol{F}^H\boldsymbol{\Gamma}_{i,1}\boldsymbol{F}\bar{\boldsymbol{r}}_1\|^2/\sigma_n^2 \\ & -\sum_{k=1}^{K_c}\sum_{i=1}^{M} \|\boldsymbol{r}_i^k - \alpha_{i,1}^{(c)}\boldsymbol{F}^H\boldsymbol{\Gamma}_{i,1}^k\boldsymbol{F}\bar{\boldsymbol{r}}_1^k\|^2/\sigma_n^2, \end{aligned} \tag{16}$$

where $\alpha_{i,1}^{(c)} = \alpha_i^{(c)}/\alpha_1^{(c)}$. $\boldsymbol{\Gamma}_{i,1}$ and $\boldsymbol{\Gamma}_{i,1}^k$ are evaluated at given $\boldsymbol{\theta}$ using (5) and (7), and their dependencies on $\boldsymbol{\theta}$ are omitted for notational simplicity. $\boldsymbol{\Gamma}_{1,1} = \boldsymbol{\Gamma}_{1,1}^k = \boldsymbol{I}_N$ and $\alpha_{1,1} = \alpha_{1,1}^{(c)} = 1$ hold by definition. As the relative amplitudes $\alpha_{i,1}$ and $\alpha_{i,1}^{(c)}$ for $i = 2, \ldots, M$ are not known *a priori* in (16), they are replaced with their ML estimates given by

$$\begin{aligned} \hat{\alpha}_{i,1} &= \mathrm{Re}\{((\boldsymbol{F}^H\boldsymbol{\Gamma}_{i,1}^H\boldsymbol{F}\boldsymbol{r}_i)^H\boldsymbol{r}_1)/(\boldsymbol{r}_1^H\boldsymbol{r}_1)\} \\ \hat{\alpha}_{i,1}^{(c)} &= \mathrm{Re}\left\{\left(\sum_{k=1}^{K_c}(\boldsymbol{F}^H(\boldsymbol{\Gamma}_{i,1}^k)^H\boldsymbol{F}\boldsymbol{r}_i^k)^H\boldsymbol{r}_1^k\right)\Big/\left(\sum_{k=1}^{K_c}(\boldsymbol{r}_1^k)^H\boldsymbol{r}_1^k\right)\right\}. \end{aligned} \tag{17}$$

Setting the partial derivatives of $Q(\boldsymbol{\theta})$ with respect to $\bar{\boldsymbol{r}}_1$ and $\bar{\boldsymbol{r}}_1^k$ to zeros, one obtains their ML estimates given by

$$\begin{aligned} \hat{\bar{\boldsymbol{r}}}_1 &= \sum_{i=1}^{M}\hat{\alpha}_{i,1}\boldsymbol{F}^H\boldsymbol{\Gamma}_{i,1}^H\boldsymbol{F}\boldsymbol{r}_i/(1+\hat{\boldsymbol{\alpha}}^T\hat{\boldsymbol{\alpha}}) \\ \hat{\bar{\boldsymbol{r}}}_1^k &= \sum_{i=1}^{M}\hat{\alpha}_{i,1}^{(c)}\boldsymbol{F}^H(\boldsymbol{\Gamma}_{i,1}^k)^H\boldsymbol{F}\boldsymbol{r}_i^k/(1+(\hat{\boldsymbol{\alpha}}^{(c)})^T\hat{\boldsymbol{\alpha}}^{(c)}), \end{aligned} \tag{18}$$

where $\hat{\boldsymbol{\alpha}} = [\hat{\alpha}_{2,1}, \ldots, \hat{\alpha}_{M,1}]^T$ and $\hat{\boldsymbol{\alpha}}^{(c)} = [\hat{\alpha}_{2,1}^{(c)}, \ldots, \hat{\alpha}_{M,1}^{(c)}]^T$ denote the estimates of relative amplitude vectors $\boldsymbol{\alpha}$ and $\boldsymbol{\alpha}^{(c)}$.

Substituting (18) into (16) and noticing that $\boldsymbol{r}_i$ and $\boldsymbol{r}_i^k$ do not depend on $\boldsymbol{\theta}$, the ML cost function in (16) can be reformulated similar to [14] as

$$Q_1(\boldsymbol{\theta}) = \arg\max_{\boldsymbol{\theta}} \boldsymbol{v}^T\boldsymbol{U}_0\boldsymbol{v}, \tag{19}$$

where $\boldsymbol{v}$ is the eigenvector of $\boldsymbol{U}_0$ corresponding to its maximal eigenvalue, and $\boldsymbol{U}_0 = \mathrm{blkdiag}(\boldsymbol{U}_1^H\boldsymbol{U}_1, \sum_{k=1}^{K_c}(\boldsymbol{U}_2^k)^H\boldsymbol{U}_2^k)$ with

$$\begin{aligned} \boldsymbol{U}_1 &= [\boldsymbol{r}_1, \boldsymbol{F}^H\boldsymbol{\Gamma}_{2,1}^H\boldsymbol{F}\boldsymbol{r}_2, \ldots, \boldsymbol{F}^H\boldsymbol{\Gamma}_{M,1}^H\boldsymbol{F}\boldsymbol{r}_M] \\ \boldsymbol{U}_2^k &= [\boldsymbol{r}_1^k, \boldsymbol{F}^H(\boldsymbol{\Gamma}_{2,1}^k)^H\boldsymbol{F}\boldsymbol{r}_2^k, \ldots, \boldsymbol{F}^H(\boldsymbol{\Gamma}_{M,1}^k)^H\boldsymbol{F}\boldsymbol{r}_M^k]. \end{aligned} \tag{20}$$

In order to maximize (19), one has to search every grid in the parameter space of $\boldsymbol{\theta}$. However, this $(M+d-1)$-dimensional parameter space is generally prohibitively large for exhaustive search from the computational efficiency perspective. A widely used and computationally much cheaper substitution to exhaustive search is GN iteration. However, GN algorithms achieve satisfactory convergence performance only when they are initialized with proper initial values, which are difficult to obtain in high-dimensional parameter spaces.

In the following, we propose a new DPD method to jointly estimate $\boldsymbol{u}$ and $\boldsymbol{\delta}$, which consists of an EM procedure for initial solution setup and a GN iteration procedure for estimate refinement. The computational complexity of the proposed DPD method is largely reduced compared to the $(M+d-1)$-dimensional exhaustive search.

B. Initial Solution Setup Using EM Method

The EM method well fits the requirement of estimating high dimensional parameter vectors [32]–[34]. It converges globally with much higher probabilities than gradient based iterative methods, such as GN and nonlinear least squares (NLS). By maximizing the auxiliary function iteratively, the cost function increases semi-monotonously [32]–[34].

In our EM model, the incomplete data is the observed signal vector denoted by $\boldsymbol{m}$, which consists of source signals and reference signals collected by all sensors, i.e., $\boldsymbol{m} = [\boldsymbol{r}^T, (\boldsymbol{r}^1)^T, \ldots, (\boldsymbol{r}^{K_c})^T]^T$, where $\boldsymbol{r} = [\boldsymbol{r}_1^T, \boldsymbol{r}_2^T, \ldots, \boldsymbol{r}_M^T]^T$, and $\boldsymbol{r}^k = [(\boldsymbol{r}_1^k)^T, (\boldsymbol{r}_2^k)^T, \ldots, (\boldsymbol{r}_M^k)^T]^T$. The parameter vector is $\boldsymbol{u}$, and the clock bias vector $\boldsymbol{\delta}$ is selected as the unobserved missing data. As a result, the complete parameter vector is $\boldsymbol{X} = [\boldsymbol{\delta}^T, \boldsymbol{m}^T]^T$. Denote by $\boldsymbol{u}^q$ the source position estimate after the qth iteration of the EM algorithm. Define [33]

$$Z(\boldsymbol{u}, \boldsymbol{u}^q) = E_{p(\boldsymbol{\delta}|\boldsymbol{u}^q, \boldsymbol{m})}\{\log p(\boldsymbol{X}; \boldsymbol{u})\}, \tag{21}$$

which is the auxiliary function that should be maximized during each iteration, where $p(\boldsymbol{\delta}|\boldsymbol{u}^q, \boldsymbol{m})$ is the conditional probability density function (pdf) of $\boldsymbol{\delta}$ given previous estimate $\boldsymbol{u}^q$ and the measurement $\boldsymbol{m}$. In the following, we evaluate this auxiliary function more concretely.

As the measurement noises of collected source signals and reference signals are uncorrelated, the log pdf of $\boldsymbol{X}$, i.e., $\log p(\boldsymbol{X}; \boldsymbol{u})$ is given as

$$\log p(\boldsymbol{X}; \boldsymbol{u}) = \log p(\boldsymbol{m}|\boldsymbol{\delta}, \boldsymbol{u}) + \log p(\boldsymbol{\delta}). \tag{22}$$

Using the ML estimate of $\bar{\boldsymbol{r}}_1$ and $\bar{\boldsymbol{r}}_1^k$, i.e., $\hat{\bar{\boldsymbol{r}}}_1$ and $\hat{\bar{\boldsymbol{r}}}_1^k$, $\log p(\boldsymbol{m}|\boldsymbol{\delta},\boldsymbol{u})$ is formulated as

$$\begin{aligned}\log p(\boldsymbol{m}|\boldsymbol{\delta},\boldsymbol{u}) = & -\sum_{i=1}^{M}\|\boldsymbol{r}_i-\hat{\alpha}_{i,1}\boldsymbol{F}^H\boldsymbol{\Gamma}_{i,1}\boldsymbol{F}\hat{\bar{\boldsymbol{r}}}_1\|^2/\sigma_n^2 \\ & -\sum_{k=1}^{K_c}\sum_{i=1}^{M}\|\boldsymbol{r}_i^k-\hat{\alpha}_{i,1}^{(c)}\boldsymbol{F}^H(\boldsymbol{\Gamma}_{i,1}^k)\boldsymbol{F}\hat{\bar{\boldsymbol{r}}}_1^k\|^2/\sigma_n^2,\end{aligned} \tag{23}$$

where $\boldsymbol{\Gamma}_{i,1}\equiv\boldsymbol{\Gamma}_{i,1}(\boldsymbol{u},\boldsymbol{\delta})$ and $\boldsymbol{\Gamma}_{i,1}^k\equiv\boldsymbol{\Gamma}_{i,1}^k(\boldsymbol{u}_k^{(c)},\boldsymbol{\delta})$ are dependent on $\boldsymbol{\delta}$ and $\boldsymbol{u}$, and $\hat{\alpha}_{i,1}$ as well as $\hat{\alpha}_{i,1}^{(c)}$ is evaluated at $\boldsymbol{\delta}$ and $\boldsymbol{u}$ using (17). $\boldsymbol{\delta}$ is assumed to be Gaussian distributed with mean $\boldsymbol{\mu}_{\boldsymbol{\delta}}$ and covariance matrix $\boldsymbol{\Sigma}$, i.e.,

$$p(\boldsymbol{\delta})=\frac{1}{(2\pi)^{\frac{M-1}{2}}|\boldsymbol{\Sigma}|^{\frac{1}{2}}}\exp\left\{-\frac{1}{2}(\boldsymbol{\delta}-\boldsymbol{\mu}_{\boldsymbol{\delta}})^T\boldsymbol{\Sigma}^{-1}(\boldsymbol{\delta}-\boldsymbol{\mu}_{\boldsymbol{\delta}})\right\}. \tag{24}$$

As $\boldsymbol{\Sigma}$ and $\boldsymbol{\mu}_{\boldsymbol{\delta}}$ are unknown, (24) is uninformative such that the conditional distribution $p(\boldsymbol{\delta}|\boldsymbol{u}^q,\boldsymbol{m})$ is also given according to (23), with $\boldsymbol{u}$ replaced by the previous estimate, $\boldsymbol{u}^q$.

Once $\log p(\boldsymbol{m},\boldsymbol{\delta};\boldsymbol{u})$ and $p(\boldsymbol{\delta}|\boldsymbol{u}^q,\boldsymbol{m})$ are obtained, the auxiliary function $Z(\boldsymbol{u},\boldsymbol{u}^q)$ can be evaluated using the Laplace approximation [35], which is detailed in the following.

Define $\boldsymbol{h}(\boldsymbol{\delta})=\log p(\boldsymbol{m}|\boldsymbol{\delta},\boldsymbol{u})+\log p(\boldsymbol{\delta})$ as the multivariate function to be integrated, $f(\boldsymbol{\delta})$ the conditional log pdf of $\boldsymbol{\delta}$ given by substituting the previous value of $\boldsymbol{u}^q$ into (23). According to [35], the integral of $\boldsymbol{h}(\boldsymbol{\delta})$ over $f(\boldsymbol{\delta})$ is given by

$$\begin{aligned}I&=\int_{\boldsymbol{\delta}}\boldsymbol{h}(\boldsymbol{\delta})\exp(f(\boldsymbol{\delta}))d\boldsymbol{\delta} \\ &\propto|-\boldsymbol{F}(\boldsymbol{\delta}^*)|^{-1/2}\boldsymbol{h}(\boldsymbol{\delta}^*)\exp(f(\boldsymbol{\delta}^*)),\end{aligned} \tag{25}$$

where $\boldsymbol{F}(\boldsymbol{\delta}^*)$ is the Hessian of $f(\boldsymbol{\delta})$ evaluated at the maximizer $\boldsymbol{\delta}^*$ of $f(\boldsymbol{\delta})$. Applying Laplace approximation to our problem yields

$$Z(\boldsymbol{u},\boldsymbol{u}^q)=\frac{p(\boldsymbol{\delta},\boldsymbol{m})}{p(\boldsymbol{m})}\boldsymbol{h}(\boldsymbol{\delta})d\boldsymbol{\delta}\propto\boldsymbol{h}(\boldsymbol{\delta}^*). \tag{26}$$

Thus the auxiliary function is developed for the considered problem.

The proposed EM algorithm proceeds as follows. In the E-step, an optimal value of $\boldsymbol{\delta}^*$ is determined by maximizing $p(\boldsymbol{\delta}|\boldsymbol{u}^q,\boldsymbol{m})$. Due to the independence between different entries of $\boldsymbol{\delta}$, this maximization procedure can be implemented via a simple one-dimensional search for each clock bias. When q is small, $\boldsymbol{u}^q$ is not accurate, and directly maximizing (23) may result in inaccurate conditional pdf of $\boldsymbol{\delta}$ and thus poor estimate of $\boldsymbol{\delta}^*$. To alleviate this problem, the simulated annealing technique [36] is applied to modify $f(\boldsymbol{\delta})$ as

$$\begin{aligned}\tilde{f}(\boldsymbol{\delta})= & -(1-\eta^{q+1})\sum_{i=2}^{M}\|\boldsymbol{r}_i-\hat{\alpha}_{i,1}\boldsymbol{F}^H\boldsymbol{\Gamma}_{i,1}\boldsymbol{F}\hat{\bar{\boldsymbol{r}}}_1\|^2/\sigma_n^2 \\ & -\sum_{k=1}^{K_c}\sum_{i=2}^{M}\|\boldsymbol{r}_i^k-\hat{\alpha}_{i,1}^{(c)}\boldsymbol{F}^H\boldsymbol{\Gamma}_{i,1}^k\boldsymbol{F}\hat{\bar{\boldsymbol{r}}}_1^k\|^2/\sigma_n^2,\end{aligned} \tag{27}$$

where $0<\eta<1$ is a predefined constant accounting for source signal weighting.

In the M-step of the EM, the auxiliary function $Z(\boldsymbol{u},\boldsymbol{u}^q)=\log p(\boldsymbol{m}|\boldsymbol{\delta}^*,\boldsymbol{u})$ is maximized to update the source position, which can be implemented via d-dimensional searching concerning $\boldsymbol{u}$. However, this procedure is computationally very expensive as it should be executed during each EM iteration. To further improve computational efficiency, sub-optimal two-step TDOA localization methods [3], [11] can be applied to yield a closed-form solution $\boldsymbol{u}^{q+1}$. Simulation results in Section VII demonstrate that this approximation yields good convergence results.

By implementing the E-step and M-step alternately, the auxiliary function $Z(\boldsymbol{u},\boldsymbol{u}^q)$ increases gradually, and reliable solutions for both $\boldsymbol{\delta}$ and $\boldsymbol{u}$ would be obtained.

C. Parameter Refinement via Gauss-Newton Iteration

When the estimates of unknown parameters converge to the close vicinity of the true solution, the EM method will converge with a much lower rate and become time consuming. This is mainly due to the fact that EM is a first-order approximation method and exhibits linear convergence rate. The GN method, on the contrary, converges with a second-order rate given proper initializations (see Chapter 9.5.3 on p. 490 in [31]). As the coarse estimate close to the true solution obtained by the EM algorithm well fits the initialization requirement of the GN method, the GN iteration could be applied to refine the coarse estimates.

In order to implement the GN iterations, we first give an equivalent formulation of the cost function in (16).

Proposition 1: The cost function in (16) is equivalent to another one given by

$$\begin{aligned}Q_2(\boldsymbol{\theta})= & -w_s\left(\sum_{i=1}^{M}\boldsymbol{U}_{1,i}\right)^H\left(\sum_{i=1}^{M}\boldsymbol{U}_{1,i}\right) \\ & -w_c\sum_{k=1}^{K_c}\left(\sum_{i=1}^{M}\boldsymbol{U}_{2,i}^k\right)^H\left(\sum_{i=1}^{M}\boldsymbol{U}_{2,i}^k\right),\end{aligned} \tag{28}$$

where $w_s>0$ and $w_c>0$ are relative weighting factors. $\boldsymbol{U}_{1,i}$ and $\boldsymbol{U}_{2,i}^k$ are the ith columns of $\boldsymbol{U}_1$ and $\boldsymbol{U}_2^k$ defined in (20), respectively. For notational simplicity, we set $w_s=1$ and $w_c=1$.

The proof of Proposition 1 is given in Appendix A.

Based on Proposition 1, the GN iteration is given by

$$\boldsymbol{\theta}^{q+1}=\boldsymbol{\theta}^q-\mathrm{Re}\left\{\boldsymbol{D}_2\right\}^{-1}\mathrm{Re}\left\{\boldsymbol{D}_1\right\}, \tag{29}$$

where $\boldsymbol{\theta}^q=[(\boldsymbol{\delta}^q)^T,(\boldsymbol{u}^q)^T]^T$ collects the estimates of the clock biases and the source position after the qth iteration, $\boldsymbol{D}_1$ and $\boldsymbol{D}_2$ are the Jacobian matrix and Hessian matrix, respectively, of $Q_2(\boldsymbol{\theta})$ evaluated at $\boldsymbol{\theta}^q$. Their detailed expressions are given by (49) and (51) in Appendix B.

Concerning the initial value setup of $\boldsymbol{\theta}^0$ for GN method, the source coordinates are obtained from the source position estimate of EM method in M-step, and the clock biases are chosen as the estimates in the E-step when the EM iteration stops.

Algorithm 1: Summary of The Proposed Dpd Algorithm.

Input : Initial source position $\boldsymbol{u}_{ini}$, measurement vector $\boldsymbol{m}$, the stopping criterion ϵ, weighting η, and the maximum iteration numbers for EM and GN iteration M_{EM} and M_{GN}.

Using EM method to obtain the coarse estimate:

$q = 0$, $\boldsymbol{u}^0 = \boldsymbol{u}_{ini}$

while $q \leq \mathrm{M}_{EM}$ **do**

The E-step: Obtaining estimate of δ_i^* by maximizing (27)

The M-step: Estimating the TDOA of source signal and then eliminating the synchronization bias using δ_i^*, then obtaining the source position $\boldsymbol{u}^{q+1}$ using closed-form solution in [11]

if $\|\boldsymbol{u}^{q+1} - \boldsymbol{u}^q\| < \epsilon$ **then**

break

end if

$q = q + 1$

end while

$\hat{\boldsymbol{u}} = \boldsymbol{u}^{q+1}$, $\boldsymbol{\delta}^* = [\delta_1^*, \delta_2^*, \ldots, \delta_{M-1}^*]^T$

Using the GN iteration to refine the coarse estimate:

$q = 0$, $\boldsymbol{\theta}^0 = [\boldsymbol{\delta}^{*T}, \hat{\boldsymbol{u}}^T]^T$

while $q \leq \mathrm{M}_{GN}$ **do**

Calculating the Jacobian and Hessian matrices using (49) and (51)

Updating the joint estimate of $\boldsymbol{\theta}$ via (29)

if $\|\boldsymbol{\theta}^{q+1} - \boldsymbol{\theta}^q\| < \epsilon$ **then**

break

end if

$q = q + 1$

end while

Return $\boldsymbol{\theta}^{q+1}$

When the sensors and the sources are not coplanar, their coordinates are further extended to 3D, i.e., $\boldsymbol{u}_i = [x_i, y_i, z_i]^T$, $\boldsymbol{u}_0 = [x, y, z]^T$, and $\boldsymbol{u}_k^{(c)} = [x_k^c, y_k^c, z_k^c]^T$. By setting $d = 3$ and using the above coordinates instead, the proposed method is extended to 3D localization straightforwardly.

A summary of the proposed source DPD method is given in Algorithm 1.

D. Computational Complexity Analysis

In this subsection, the computational complexity of the proposed DPD method is analyzed. This complexity is also compared with that of exhaustive search DPD method and the two-step methods.

Denote by N_{EM} the number of EM iterations, N_δ the number of candidates for searching δ_i^*. The execution of E step using (27) mainly involves FFT and inverse FFT operations, with a computational complexity of $\mathcal{O}(N \log_2 N)$, and the complexity of M step is $\mathcal{O}(M^3)$, which can be neglected because $M \ll N$. Therefore, the computational complexity of the EM method is approximately $\mathcal{O}((M-1)^2(K_c+1)N_\delta N_{EM} N \log_2 N)$. For the GN iterations, the computational complexity mainly concentrates on the calculation of first- and second-order partial derivative matrices in (49) and (51), which is given by $\mathcal{O}(N \log_2 N)$. Typically a maximum of 10 iterations are enough for the GN iteration to converge, thus the GN iteration has a computational complexity of $\mathcal{O}(N \log_2 N)$. Combining the above analysis results, the overall computational complexity of the proposed method is approximately given by $\mathcal{O}((M-1)^2(K_c+1)N_\delta N_{EM} N \log_2 N)$, which is dominated by the complexity of EM method.

Next the computational complexity of the exhaustive search DPD method given in (19) is shown. Without loss of generality, assume that the search range and search interval along each coordinate axis are given by D_x and d_x, respectively. Moreover, the search range for δ_i is D_δ with search interval given by d_δ. The intervals d_x and d_δ can be determined according to their CRLBs given in Section V. Then a total of approximately $N_{grid} = \lceil \frac{D_x}{d_x} \rceil^d \lceil \frac{D_\delta}{d_\delta} \rceil^{M-1}$ grid points should be searched, with the computational complexity corresponding to each grid point given by $\mathcal{O}((M-1)(K_c+1)N \log_2 N)$. Thus the total complexity of exhaustive search is approximately $\mathcal{O}(N_{grid}(M-1)(K_c+1)N \log_2 N)$. As N_{grid} increases exponentially with increased M and d, the computational load of exhaustive search is prohibitively larger than that of the proposed method, which renders it impractical to be applied.

On the other hand, the two-step methods estimate the signal TDOAs of source $\boldsymbol{u}_0$ and anchor sources with a complexity of $\mathcal{O}((M-1)(K_c+1)N \log_2 N)$. In the second step, calibrating the clock biases and solving the source position using the calibrated TDOAs require a computational complexity of approximately $\mathcal{O}(M^3)$, which is mainly involved in matrix inversion. Therefore, the two-step methods are computationally much more efficient than the proposed method with a complexity of $\mathcal{O}((M-1)(K_c+1)N \log_2 N + M^3)$ at the cost of yielding suboptimal solutions.

V. CRLB

Although there have been some works focused on CRLB derivation for synchronous TDOA-based DPD localization [37] and asynchronous two-step localization scenarios [28], there exist no CRLB derivations for the considered problem from a DPD perspective. In this section, we derive the CRLB for the source DPD problem in asynchronous sensor networks using active anchor sources.

The parameter set consists of the real parts and imaginary parts of noiseless signals received by the first sensor, the relative amplitudes $\alpha_{i,1}$ and $\alpha_{i,1}^{(c)}$, the non-redundant clock biases δ_i and the source location $\boldsymbol{u}$. With slight abuse of notations, define the composite parameter vector as $\boldsymbol{\theta} = [\mathrm{Re}\{\boldsymbol{y}_1\}^T, \mathrm{Im}\{\boldsymbol{y}_1\}^T, (\boldsymbol{y}^{(c)})^T, \boldsymbol{\alpha}^T, (\boldsymbol{\alpha}^{(c)})^T, \boldsymbol{\delta}^T, (\boldsymbol{u})^T]^T$ where $\boldsymbol{y}_1$ denotes the unknown source signal, and

$$\boldsymbol{y}^{(c)} = [\boldsymbol{Y}_1^T, \ldots, \boldsymbol{Y}_{K_c}^T]^T,$$

with $\boldsymbol{Y}_i = [\mathrm{Re}\{(\boldsymbol{y}_i^{(c)})\}^T, \mathrm{Im}\{(\boldsymbol{y}_i^{(c)})\}^T]^T$ containing the real and imaginary parts of the unknown anchor source signals.

The CRLB is obtained by calculating the inverse of the Fisher information matrix (FIM) [38], with the FIM obtained by

$$FIM(\boldsymbol{\theta}) = \frac{2}{\sigma_n^2}\mathrm{Re}\{\boldsymbol{V}^H\boldsymbol{V}\}, \tag{30}$$

where $\boldsymbol{V} = \frac{\partial \boldsymbol{m}}{\partial \boldsymbol{\theta}}$ is the partial derivative matrix of the measurement vector w.r.t. the composite parameter vector. After some manipulations, the FIM is given by

$$FIM(\boldsymbol{\theta}) = \frac{2}{\sigma_n^2}\begin{bmatrix} \boldsymbol{A} & \mathrm{Re}\{\boldsymbol{B}\} \\ \mathrm{Re}\{\boldsymbol{B}\}^T & \mathrm{Re}\{\boldsymbol{C}\} \end{bmatrix}, \tag{31}$$

where $\boldsymbol{A}$ is a $2N(K_c+1)\times 2N(K_c+1)$ block diagonal matrix given by

$$\boldsymbol{A} = \mathrm{blkdiag}\left(\boldsymbol{I}_{2N}\sum_{i=1}^{M}\alpha_{i,1}^2, \boldsymbol{I}_{2NK_c}\sum_{i=1}^{M}(\alpha_{i,1}^{(c)})^2\right), \tag{32}$$

where $\alpha_{1,1}=1$ and $\alpha_{1,1}^{(c)}=1$. The matrix $\boldsymbol{B}$ in the FIM is given by

$$\boldsymbol{B} = \begin{bmatrix} \boldsymbol{B}_1 & \boldsymbol{O}_{N\times(M-1)} & \boldsymbol{B}_2 & \boldsymbol{B}_3 \\ -j\boldsymbol{B}_1 & \boldsymbol{O}_{N\times(M-1)} & -j\boldsymbol{B}_2 & -j\boldsymbol{B}_3 \\ \boldsymbol{O}_{N\times(M-1)} & \boldsymbol{B}_4^1 & \boldsymbol{B}_5^1 & \boldsymbol{O}_{N\times d} \\ \boldsymbol{O}_{N\times(M-1)} & -j\boldsymbol{B}_4^1 & -j\boldsymbol{B}_5^1 & \boldsymbol{O}_{N\times d} \\ \vdots & \vdots & \vdots & \vdots \\ \boldsymbol{O}_{N\times(M-1)} & \boldsymbol{B}_4^{K_c} & \boldsymbol{B}_5^{K_c} & \boldsymbol{O}_{N\times d} \\ \boldsymbol{O}_{N\times(M-1)} & -j\boldsymbol{B}_4^{K_c} & -j\boldsymbol{B}_5^{K_c} & \boldsymbol{O}_{N\times d} \end{bmatrix}, \tag{33}$$

where d is the dimension of the considered scenario, and

$$\begin{aligned} \boldsymbol{B}_1 &= [\alpha_{2,1}\boldsymbol{y}_1, \ldots, \alpha_{M,1}\boldsymbol{y}_1] \\ \boldsymbol{B}_2 &= [\alpha_{2,1}^2\boldsymbol{b}, \cdots, \alpha_{M,1}^2\boldsymbol{b}] \\ \boldsymbol{B}_3 &= \sum_{i=2}^{M}\alpha_{i,1}^2\boldsymbol{b}(\boldsymbol{\rho}_i-\boldsymbol{\rho}_1)^T \\ \boldsymbol{B}_4^k &= [\alpha_{2,1}^{(c)}\boldsymbol{y}_k^{(c)}, \ldots, \alpha_{M,1}^{(c)}\boldsymbol{y}_k^{(c)}] \\ \boldsymbol{B}_5^k &= [(\alpha_{2,1}^{(c)})^2\boldsymbol{b}^k, \ldots, (\alpha_{M,1}^{(c)})^2\boldsymbol{b}^k], \end{aligned} \tag{34}$$

where $\boldsymbol{b} = \boldsymbol{F}^H\tilde{\boldsymbol{n}}\boldsymbol{F}\boldsymbol{y}_1$, $\boldsymbol{b}^k = \boldsymbol{F}^H\tilde{\boldsymbol{n}}\boldsymbol{F}\boldsymbol{y}_k^{(c)}$, with $\tilde{\boldsymbol{n}} = j\frac{2\pi f_s}{Nc}\mathrm{Diag}(\boldsymbol{n})$. The matrix $\boldsymbol{C}$ in (31) is given by

$$\boldsymbol{C} = \begin{bmatrix} \boldsymbol{C}_1 & \boldsymbol{C}_2 \\ \boldsymbol{C}_2^H & \boldsymbol{C}_3 \end{bmatrix}, \tag{35}$$

where

$$\begin{aligned} \boldsymbol{C}_1 &= \mathrm{blkdiag}\left(\boldsymbol{y}_1^H\boldsymbol{y}_1\boldsymbol{I}_{M-1}, \sum_{k=1}^{K_c}(\boldsymbol{y}_k^{(c)})^H(\boldsymbol{y}_k^{(c)})\boldsymbol{I}_{M-1}\right) \\ \boldsymbol{C}_2 &= [\boldsymbol{C}_{2,1}^T, \boldsymbol{C}_{2,2}^T]^T \\ \boldsymbol{C}_{2,1} &= [\mathrm{Diag}(\boldsymbol{\alpha})\boldsymbol{y}_1^H\boldsymbol{b}, [\alpha_{2,1}\boldsymbol{y}_1^H\boldsymbol{b}(\boldsymbol{\rho}_2-\boldsymbol{\rho}_1), \\ &\qquad \ldots, \alpha_{M,1}\boldsymbol{y}_1^H\boldsymbol{b}(\boldsymbol{\rho}_M-\boldsymbol{\rho}_1)]^T] \\ \boldsymbol{C}_{2,2} &= \left[\sum_{k=1}^{K_c}(\boldsymbol{y}_k^{(c)})^H\boldsymbol{b}^k\mathrm{Diag}(\boldsymbol{\alpha}^{(c)}), \boldsymbol{O}_{(M-1)\times d}\right] \\ \boldsymbol{C}_3 &= \begin{bmatrix} \boldsymbol{D}_1 & \boldsymbol{D}_2 \\ \boldsymbol{D}_2^H & \boldsymbol{D}_3 \end{bmatrix}, \end{aligned} \tag{36}$$

where with slight abuse of notations, the matrices $\boldsymbol{D}_1$, $\boldsymbol{D}_2$ and $\boldsymbol{D}_3$ are given by

$$\begin{aligned} \boldsymbol{D}_1 &= \mathrm{Diag}\left(\left[\alpha_{2,1}^2\tilde{\boldsymbol{s}} + \sum_{k=1}^{K_c}(\alpha_{2,1}^{(c)})^2\tilde{\boldsymbol{s}}^k \right. \right. \\ &\qquad \left. \left. \ldots, \alpha_{M,1}^2\tilde{\boldsymbol{s}} + \sum_{k=1}^{K_c}(\alpha_{M,1}^{(c)})^2\tilde{\boldsymbol{s}}^k\right]^T\right) \\ \boldsymbol{D}_2 &= \tilde{\boldsymbol{s}}\begin{bmatrix} \alpha_{2,1}^2(\boldsymbol{\rho}_2-\boldsymbol{\rho}_1)^T \\ \vdots \\ \alpha_{M,1}^2(\boldsymbol{\rho}_M-\boldsymbol{\rho}_1)^T \end{bmatrix} \\ \boldsymbol{D}_3 &= \tilde{\boldsymbol{s}}\sum_{i=1}^{M}\alpha_{i,1}^2(\boldsymbol{\rho}_i-\boldsymbol{\rho}_1)(\boldsymbol{\rho}_i-\boldsymbol{\rho}_1)^T, \end{aligned} \tag{37}$$

where $\tilde{\boldsymbol{s}} = \boldsymbol{y}_1^H\boldsymbol{F}^H\tilde{\boldsymbol{n}}^H\tilde{\boldsymbol{n}}\boldsymbol{F}\boldsymbol{y}_1$, $\tilde{\boldsymbol{s}}^k = (\boldsymbol{y}_k^{(c)})^H\boldsymbol{F}^H\tilde{\boldsymbol{n}}^H\tilde{\boldsymbol{n}}\boldsymbol{F}\boldsymbol{y}_k^{(c)}$.

Upon obtaining the FIM matrix in (31), using the Schur-complementary theorem in [39], the FIM of $\boldsymbol{\alpha}$, $\boldsymbol{\alpha}^{(c)}$, $\boldsymbol{\delta}$ and $\boldsymbol{u}$ can be obtained as

$$FIM = \frac{2}{\sigma_n^2}\left(\mathrm{Re}\{\boldsymbol{C}\} - \mathrm{Re}\{\boldsymbol{B}\}^T\boldsymbol{A}^{-1}\mathrm{Re}\{\boldsymbol{B}\}\right). \tag{38}$$

This result is different from the one derived in [40]. The complementary part $\mathrm{Re}\{\boldsymbol{B}\}^T\boldsymbol{A}^{-1}\mathrm{Re}\{\boldsymbol{B}\}$ is included and it is not proportional to $\mathrm{Re}\{\boldsymbol{C}\}$. Combining the facts that $\mathrm{Re}\{\boldsymbol{y}_1^H\boldsymbol{b}\}=0$, $\mathrm{Re}\{(\boldsymbol{y}_k^{(c)})^H\boldsymbol{b}^k\}=0$, and after some straightforward mathematical calculations, (38) can be simplified as

$$FIM = \frac{2}{\sigma_n^2}\begin{bmatrix} \boldsymbol{\Lambda} & \boldsymbol{O}_{2(M-1)\times M-1} & \boldsymbol{O}_{2(M-1)\times d} \\ \boldsymbol{O}_{M-1\times 2(M-1)} & \tilde{s}\boldsymbol{\Upsilon} + \sum_{k=1}^{K_c}\tilde{s}^k\boldsymbol{\Upsilon}^{(c)} & \tilde{s}\boldsymbol{\Upsilon}\boldsymbol{\rho} \\ \boldsymbol{O}_{d\times 2(M-1)} & \tilde{s}\boldsymbol{\rho}^T\boldsymbol{\Upsilon} & \tilde{s}\boldsymbol{\rho}^T\boldsymbol{\Upsilon}\boldsymbol{\rho} \end{bmatrix}, \tag{39}$$

where $\boldsymbol{\Lambda} = \mathrm{blkdiag}\left(\|\boldsymbol{y}_1\|^2\left(\boldsymbol{I}_{M-1} - \frac{\boldsymbol{\alpha}\boldsymbol{\alpha}^T}{a_1}\right), \sum_{k=1}^{K_c}\|\boldsymbol{y}_k^{(c)}\|^2\left(\boldsymbol{I}_{M-1} - \frac{\boldsymbol{\alpha}^{(c)}(\boldsymbol{\alpha}^{(c)})^T}{a_2}\right)\right)$, $\boldsymbol{\Upsilon} = \tilde{\boldsymbol{\alpha}}^2 - \frac{\tilde{\boldsymbol{\alpha}}\boldsymbol{\alpha}\boldsymbol{\alpha}^T\tilde{\boldsymbol{\alpha}}}{a_1}$, $\boldsymbol{\Upsilon}^{(c)} = (\tilde{\boldsymbol{\alpha}}^{(c)})^2 - \frac{\tilde{\boldsymbol{\alpha}}^{(c)}\boldsymbol{\alpha}^{(c)}(\boldsymbol{\alpha}^{(c)})^T\tilde{\boldsymbol{\alpha}}^{(c)}}{a_2}$, $\boldsymbol{\rho} = [\boldsymbol{\rho}_2-\boldsymbol{\rho}_1, \ldots, \boldsymbol{\rho}_M-\boldsymbol{\rho}_1]^T$, where $\tilde{\boldsymbol{\alpha}} = \mathrm{Diag}(\boldsymbol{\alpha})$, $\tilde{\boldsymbol{\alpha}}^{(c)} = \mathrm{Diag}(\boldsymbol{\alpha}^{(c)})$, $a_1 = 1+\boldsymbol{\alpha}^T\boldsymbol{\alpha}$ and $a_2 =$

$1+(\boldsymbol{\alpha}^{(c)})^T\boldsymbol{\alpha}^{(c)}$. It is worth mentioning that the FIM in (39) is block diagonal, which indicates that the amplitude vectors $\boldsymbol{\alpha}$ and $\boldsymbol{\alpha}^{(c)}$ are not coupled with $\boldsymbol{\delta}$ and $\boldsymbol{u}$. Therefore, the CRLB of $\boldsymbol{\delta}$ and $\boldsymbol{u}$ can be obtained by calculating the inverse of the lower right part of (39).

VI. Influence Analysis of Anchor Sources on DPD performance

In this section, the effects of anchor source number and anchor source positions on the performance of the proposed DPD method are analyzed. The analysis starts with the formulation of the derived CRLB in Section V, with the relative amplitudes $\boldsymbol{\alpha}$ and $\boldsymbol{\alpha}^{(c)}$ assumed to be all-one vectors for notational simplicity. It should be noted that the conclusions made in this section can also be extended easily to general cases with arbitrary $\boldsymbol{\alpha}$ and $\boldsymbol{\alpha}^{(c)}$.

In the absence of anchor sources, i.e., $K_c=0$, $\boldsymbol{B}$ in (33) degenerates into

$$\boldsymbol{B}=\begin{bmatrix}\boldsymbol{B}_1 & \boldsymbol{B}_2 & \boldsymbol{B}_3\\ -j\boldsymbol{B}_1 & -j\boldsymbol{B}_2 & -j\boldsymbol{B}_3\end{bmatrix},$$

and the matrix $\boldsymbol{C}$ in (35) degenerates into

$$\boldsymbol{C}=\begin{bmatrix}\|\boldsymbol{y}_1\|^2\boldsymbol{I}_{M-1} & \boldsymbol{O}_{M-1} & \boldsymbol{O}_{M-1\times d}\\ \boldsymbol{O}_{M-1} & \tilde{s}\boldsymbol{I}_{M-1} & \tilde{s}\boldsymbol{\rho}\\ \boldsymbol{O}_{d\times M-1} & \tilde{s}\boldsymbol{\rho}^T & \tilde{s}\boldsymbol{\rho}^T\boldsymbol{\rho}\end{bmatrix}.$$

After some manipulations the FIM corresponding to $\boldsymbol{\alpha}$, $\boldsymbol{\delta}$ and $\boldsymbol{u}$ is given by

$$FIM_0(\boldsymbol{\alpha},\boldsymbol{\delta},\boldsymbol{u})=\frac{2}{\sigma_n^2}\begin{bmatrix}\|\boldsymbol{y}_1\|^2\boldsymbol{P} & \boldsymbol{O}_{M-1} & \boldsymbol{O}_{M-1\times 2}\\ \boldsymbol{O}_{M-1} & \tilde{s}\boldsymbol{P} & \tilde{s}\boldsymbol{P}\boldsymbol{\rho}\\ \boldsymbol{O}_{2\times M-1} & \tilde{s}\boldsymbol{\rho}^T\boldsymbol{P} & \tilde{s}\boldsymbol{\rho}^T\boldsymbol{P}\boldsymbol{\rho}\end{bmatrix},\tag{40}$$

where $\boldsymbol{P}=\boldsymbol{I}_{M-1}-\frac{\boldsymbol{1}\boldsymbol{1}^T}{M}$ is an invertible positive definite matrix. The matrix $FIM_0(\boldsymbol{\alpha},\boldsymbol{\delta},\boldsymbol{u})$ is not invertible because it is rank-deficient. Therefore, when no anchor sources are present, the localization problem is under-determined. This conclusion is very intuitive. Using the signals received at M sensors, at most $M-1$ non-redundant TDOA measurements can be obtained while there are $M+d-1>M-1$ unknown parameters to estimate, whose solutions are not unique.

When there are $K_c>0$ anchor sources available, the corresponding FIM matrix with respect to $\boldsymbol{\delta}$ and $\boldsymbol{u}$ can be obtained by substituting $\boldsymbol{\alpha}=\boldsymbol{1}$ and $\boldsymbol{\alpha}^{(c)}=\boldsymbol{1}$ into (39), which yields

$$FIM_{K_c}(\boldsymbol{\delta},\boldsymbol{u})=\frac{2}{\sigma_n^2}\begin{bmatrix}(\tilde{s}+\sum_{k=1}^{K_c}\tilde{s}^k)\boldsymbol{P} & \tilde{s}\boldsymbol{P}\boldsymbol{\rho}\\ \tilde{s}\boldsymbol{\rho}^T\boldsymbol{P} & \tilde{s}\boldsymbol{\rho}^T\boldsymbol{P}\boldsymbol{\rho}\end{bmatrix}.\tag{41}$$

In this case, $FIM_{K_c}(\boldsymbol{\delta},\boldsymbol{u})$ is no longer rank deficient for any nonzero K_c due to the presence of the term $\sum_{k=1}^{K_c}\tilde{s}^k$. The source position can be uniquely determined with nonzero K_c. To gain deeper insights, using the Schur-complementary theorem again, the FIM of $\boldsymbol{u}$ is given by

$$FIM_{K_c}(\boldsymbol{u})=\frac{2}{\sigma_n^2}\left(\tilde{s}-\frac{\tilde{s}^2}{\tilde{s}+\sum_{k=1}^{K_c}\tilde{s}^k}\right)\boldsymbol{\rho}^T\boldsymbol{P}\boldsymbol{\rho}.\tag{42}$$

Obviously, the eigenvalues of $FIM_{K_c}(\boldsymbol{u})$ increase monotonically with increased K_c, and thus the localization precision improves when more anchor sources are available. The explanation for this is also very intuitive. When K_c increases, the eigenvalues of the FIM of $\boldsymbol{\delta}$, i.e., $\frac{2}{\sigma_n^2}(\tilde{s}+\sum_{k=1}^{K_c}\tilde{s}^k)\boldsymbol{P}$ increase, which results in higher accuracy of clock bias estimates. As $\boldsymbol{\delta}$ and $\boldsymbol{u}$ are coupled, improved estimate of $\boldsymbol{\delta}$ leads to more accurate estimate of $\boldsymbol{u}$.

Moreover, note that $\tilde{s}$ and $\tilde{s}^k$ are proportional to the SNR. When the SNR of the source $\boldsymbol{u}_0$ is fixed and the SNR of the anchor sources is far smaller than it, i.e., $\tilde{s}^k\ll\tilde{s}$, $FIM_{K_c}(\boldsymbol{u})$ in (42) approaches $\boldsymbol{O}_{d\times d}$ and the localization precision degrades significantly. On the contrary, when $\tilde{s}^k\gg\tilde{s}$, $FIM_{K_c}(\boldsymbol{u})$ in (42) can be approximated by $2\tilde{s}\boldsymbol{\rho}^T\boldsymbol{P}\boldsymbol{\rho}/\sigma_n^2$, which is in fact the FIM of $\boldsymbol{u}$ in synchronous sensor networks where clock biases are absent.

To conclude, in order to uniquely determine the source position in asynchronous sensor networks, at least one anchor source is required. As the number of anchor sources increases, the localization performance improves consistently. Moreover, *anchor source positions cast no effects on localization precision*, which is due to the fact that sensors are assumed to be accurately deployed [4].

TABLE II
Coordinates of Sensors (in Meters)

sensor no.i	x_i	y_i	sensor no.i	x_i	y_i
1	-1000	-1000	4	1000	-1000
2	-1000	1000	5	1000	1000
3	0	1000			

VII. Simulation Results

In this section, numerical simulations are conducted to validate the effectiveness of the proposed DPD method. The source of interest is located at $\boldsymbol{u}_0=[0,0]^T$ m. There are three anchor sources with their stationary positions given by $\boldsymbol{u}_1^{(c)}=[50,-50]^T$ m, $\boldsymbol{u}_2^{(c)}=[-100,80]^T$ m and $\boldsymbol{u}_3^{(c)}=[150,-200]^T$ m, respectively. However, in the first, the second and the third simulations, only the first two anchor sources are used. A total of $M=5$ sensors are used and their locations are given in Table II. The clock biases are given by $\delta_1=200$ m, $\delta_2=-100$ m, $\delta_3=-500$ m and $\delta_4=300$ m, respectively. Without loss of generality, the source signal and reference signals are linear frequency modulated. The bandwidth of source signal is $B_s=100$ KHz and the bandwidth of reference signals is $B_c=50$ KHz. The sampling rate is $f_s=600$ KHz with the sample number given by $N=1500$. As the noise variance remains the same for all sensors, the SNR is proportional to the squared amplitude of signal envelope. Without loss of generality, the SNR is defined in terms of the source signal collected by the first

sensor, i.e., $\boldsymbol{r}_1$. The relative amplitude vector of received source signal is $\boldsymbol{\alpha} = [0.8, 1.1, 0.8, 0.9]^T$ and the relative amplitude vector of reference signals is determined such that the SNR of $\boldsymbol{r}_i$ is 3 dB higher than that of $\boldsymbol{r}_i^k$. For each simulation, a total of 2000 Monte-Carlo runs are used to yield the statistical results. Similar to [20], two criteria are applied to evaluate the performance of different methods since the proposed method does not guarantee global convergence. The first criterion is the commonly used RMSE and the second is the cumulative density function (CDF) of estimation error. The former evaluates the local performance in the vicinity of real solution while the latter evaluates its global performance.

First, the negative effects of clock biases on localization RMSE are shown. In Fig. 2, the curves of localization RMSE with different levels of clock biases as well as the theoretical CRLB curves are plotted for varying SNRs. Without loss of generality, all clock biases are set to be equal for illustration purposes, although the proposed method does not require them to be equal or their statistical distribution be known. As depicted in Fig. 2, the localization performance is deteriorated and the localization bias caused by clock biases dominates in the localization error. The CRLB for the proposed DPD with clock biases present is about 3 dB higher than the CRLB for synchronized DPD where clock biases are absent.

In the first simulation, the performance of the proposed method is examined. The conventional two-step localization method and the DPD method using GN iteration only (termed GN DPD in the following) are simulated for comparison. It should be mentioned that the classic DPD methods in [14], [15], [17] are not designed for time delay based source positioning in asynchronous sensor networks, they are not implemented here for comparison. The exhaustive search based DPD estimator in (19) is not shown because it is computationally prohibitive. For the two-step method, TDOAs are estimated using ML-based generalized cross-correlation (GCC) method, then the method in [28] is used to estimate clock biases, which is followed by the method in [11] to solve the source position using calibrated TDOAs. For our proposed method, $\eta = 0.8$, $\epsilon = 1$, $M_{EM} = 50$ and $M_{GN} = 10$. Also, the theoretical CRLB derived in Section V is plotted. The initial solution for the GN DPD and the proposed DPD methods is selected randomly within a squared region of 900 m $\times$ 900 m around the source position $\boldsymbol{u}_0$ for each Monte-Carlo simulation.

In Fig. 3 and Fig. 4, the localization RMSE curves and the clock bias estimation RMSE curves of different methods are plotted as a function of SNR. As depicted in both figures, the two-step method is suboptimal. It approaches the CRLB gradually as SNR increases, but cannot reach it. The GN DPD method converges to local optimum for about 80% of ensemble runs. Consequently, GN DPD is corrupted by large localization bias and it cannot reach the CRLB at any SNRs. On the contrary, the proposed DPD can reach the CRLB at a lower SNR threshold (10 dB) than the two-step methods. The reason accounting for its deviation from the CRLB under lower SNR (SNR $<$ 10 dB) is that it may also converge to local optimums with a small probability caused by large noise.

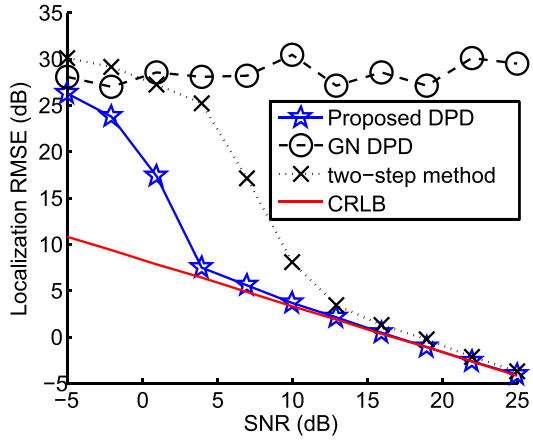

Fig. 3. Localization RMSE curves of different methods versus SNR. $K_c = 2$. $f_s = 600$ KHz, $N = 1500$.

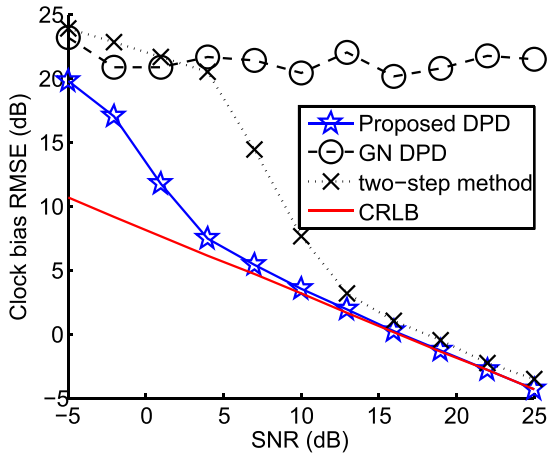

Fig. 4. Clock bias RMSE curves of different methods versus SNR. $K_c = 2$. $f_s = 600$ KHz, $N = 1500$.

In Fig. 5 and Fig. 6, the CDF criterion is applied to evaluate the estimation error distributions of source location and clock biases of each method. SNR is fixed to 10 dB. Other setting remains the same as that in Fig. 3. As shown in Fig. 5 and Fig. 6, the proposed method outperforms the other two methods. The GN DPD method, although could yield relatively accurate solutions when converging to global optimums, has more than 70% probability of local convergence.

In the second simulation, the sensors are deployed randomly within a square of 1000 m $\times$ 1000 m around the origin while other configurations remain the same as that produces Fig. 5. Fig. 7 and Fig. 8 provide the localization error CDF curves of different methods. Similarly, the tremendous performance improvement of the proposed method in estimation accuracy compared with the conventional two-step method could be observed. Moreover, the global convergence rate of the proposed method is greatly improved compared with the GN DPD method.

In the third simulation, the SNR is fixed to 10 dB and the sensor are deployed as given in Table II. Different w_s and w_c

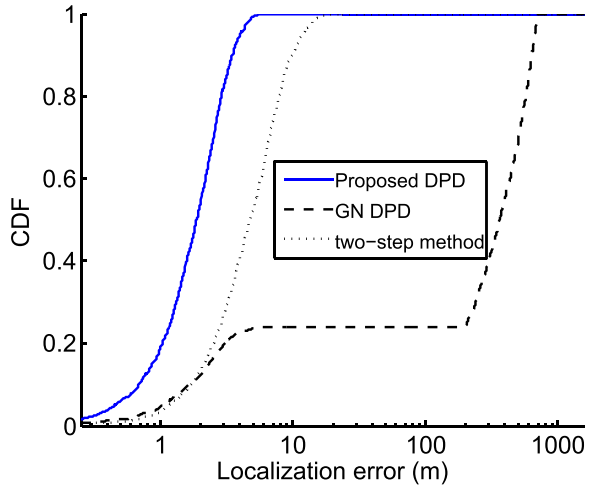

Fig. 5. Localization error CDF curves of different methods with SNR = 10 dB.

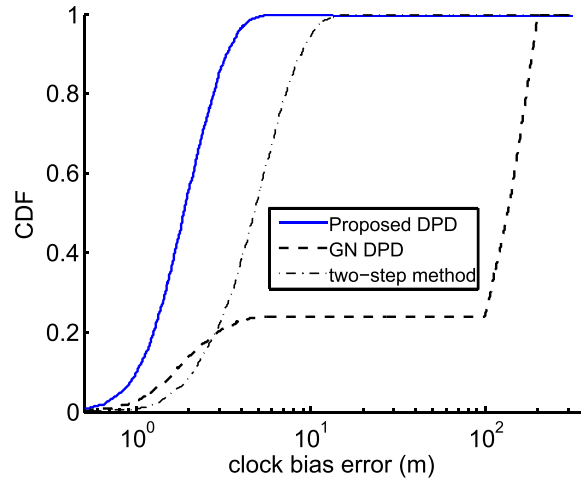

Fig. 6. Clock bias estimation error CDF curves of different methods with SNR = 10 dB.

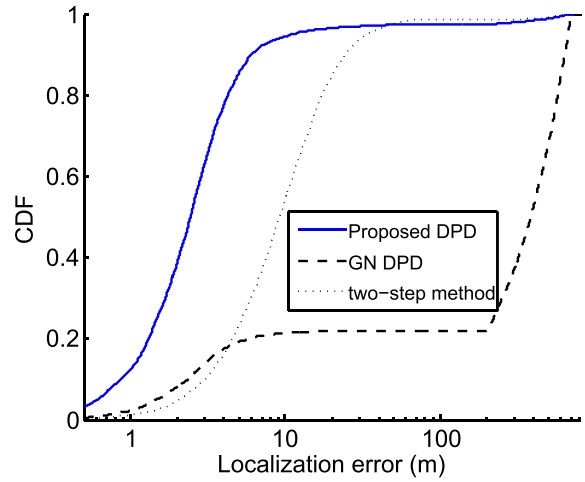

Fig. 7. Localization error CDF curves of different methods with SNR = 10 dB.

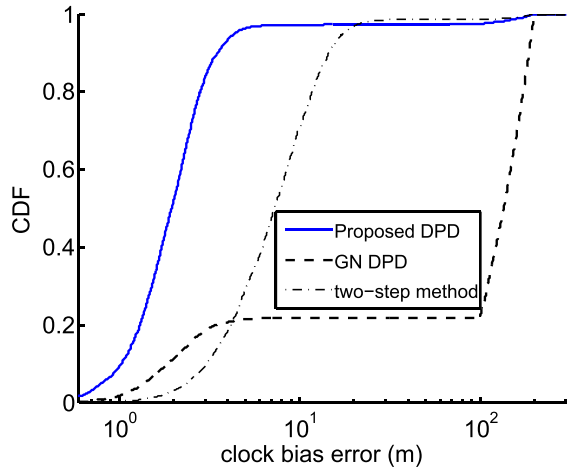

Fig. 8. Clock bias estimation error CDF curves of different methods with SNR = 10 dB.

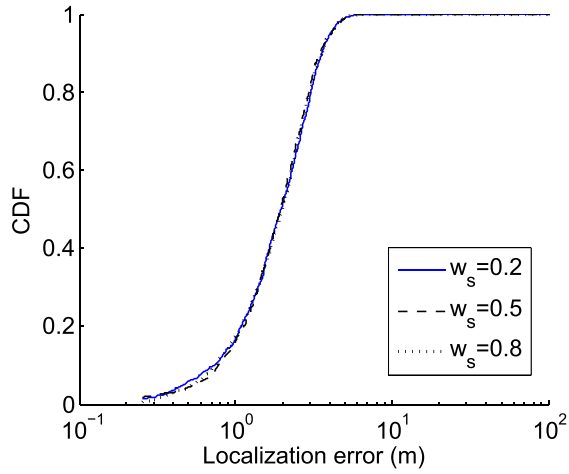

Fig. 9. Localization error CDF curves of the proposed method using different relative weighting factors. SNR = 10 dB. $K_c = 2$.

combinations are used to validate the conclusion in Proposition 1. w_s varies from 0.2 to 0.8 with w_c determined by $w_s + w_c = 1$. In Fig. 9, the localization error CDF curves of the proposed DPD method using different w_s values are plotted. The corresponding clock bias estimation error CDF curves are also shown in Fig. 10. As depicted in Fig. 9 and Fig. 10, the three curves with different w_s values are consistent. Therefore, the localization performance of the proposed method is insensitive to the relative weighting and the conclusion in Proposition 1 is validated.

In the fourth simulation, the effects of the number of anchor sources on localization performance are shown. In Fig. 11 and Fig. 12, the localization RMSEs and the clock bias estimation RMSEs of the proposed method with varying anchor source numbers are plotted as a function of SNR. From Fig. 11 and Fig. 12, one can find that as the number of anchor sources increases, the localization performance improves consistently. Particularly, with only one anchor source present, the proposed method could not approach the CRLB until the SNR exceeds

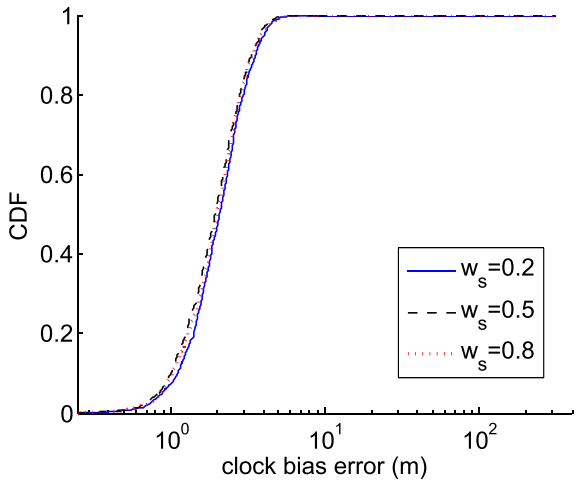

Fig. 10. Clock bias estimation error CDF curves of the proposed method using different relative weighting factor w_i. SNR $= 10$ dB. $K_c = 2$.

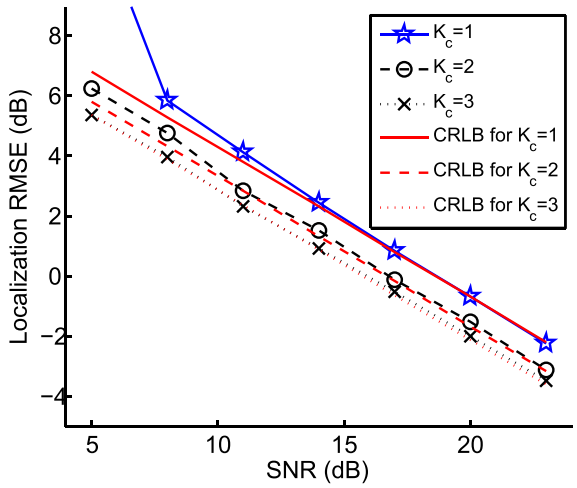

Fig. 11. Localization RMSE curves of the proposed DPD method. The number of anchor sources varies from 1 to 3. $f_s = 600$ KHz, $N = 1500$.

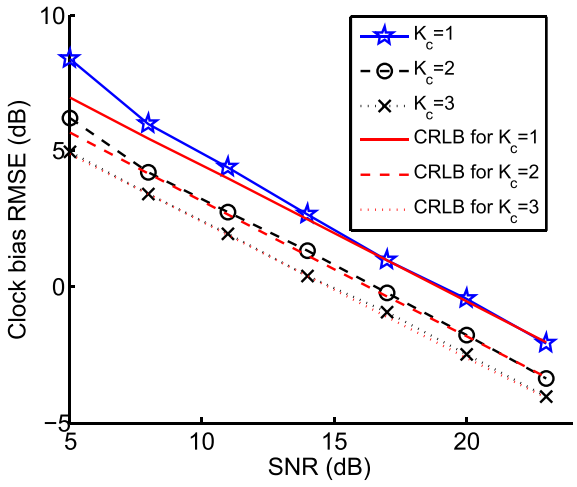

Fig. 12. Clock bias RMSE curves of the proposed DPD method. The number of anchor sources varies from 1 to 3. $f_s = 600$ KHz, $N = 1500$.

TABLE III
COMPARISON OF THE NUMBER OF MULTIPLICATIONS FOR DIFFERENT METHODS

N	1000	1500	2000
Grid search	106×10^{18}	562×10^{18}	1835×10^{18}
Proposed DPD	7×10^{8}	11×10^{8}	16×10^{8}
Two-step	12×10^{4}	19×10^{4}	26×10^{4}

15 dB. This SNR threshold reduces to about 8 dB when there are two anchor sources. When there are three anchor sources, the proposed method can reach the CRLB for all simulated SNRs. This phenomenon is consistent with our conclusions in Section VI, which indicate that more anchor sources could lead to more accurate clock bias estimates and thus improved localization performance.

Last, the numerical comparison of the computational complexity of different methods is shown in terms of the number of multiplication operations under varying signal sample numbers. SNR $= 10$ dB. For the exhaustive search based DPD method, the search range is given by $D_x = 2000$ m and the search interval d_x is determined according to the root CRLB for $\boldsymbol{u}$. The search range for clock bias is given by $D_\delta = 500$ m, and its search interval d_δ is determined by the root CRLB of $\boldsymbol{\delta}$. For the proposed method, N_δ is set to 20, $N_{EM} = 50$, and $N_{GN} = 10$. The results are computed using the theoretical analyses given in Section IV-D, and they are shown in Table III. As shown in Table III, the proposed method could still guarantee real-time processing, although it requires much longer computational time compared with the conventional two-step method, which is mainly due to the repeated signal correlation operations for each candidate of δ_i during each EM iteration. Meanwhile, the computational complexity of the proposed method is reduced tremendously compared with exhaustive search based DPD method, which is usually computationally prohibitive.

VIII. CONCLUSION

In this paper, the TDOA-based source DPD problem in asynchronous sensor networks was studied. The clock biases were demonstrated via theoretical analyses to make localization results biased if they were neglected, which highlighted the necessity of joint source position estimation and clock bias calibration. We then proposed a DPD method integrating the EM and GN iterations to realize computationally efficient source localization in asynchronous sensor networks. The corresponding CRLB was derived, and the influence of anchor sources on the performance of the proposed DPD method was also analyzed. Numerical results demonstrated that the proposed method achieved higher localization accuracy than conventional two-step methods and exhibited much higher global convergence rate than the GN DPD method. It could approach the CRLB under mild conditions with acceptable computational complexity. As the number of anchor sources increased, the localization performance further improved. Besides being inherently suitable for TOA-based source positioning, the rationale behind the proposed method

could also be applied to calibrate the frequency bias or array manifold bias in FDOA or AOA based source DPD problems with proper modifications, which are left for future researches.

APPENDIX A
PROOF OF PROPOSITION 1

In this appendix, proof of Proposition 1 is given. The original cost function to be maximized can be rewritten as

$$\begin{aligned} Q_3(\boldsymbol{\theta}) = & -\sum_{i=2}^{M} \|\boldsymbol{r}_i - \hat{\alpha}_{i,1}\boldsymbol{F}^H\boldsymbol{\Gamma}_{i,1}\boldsymbol{F}\bar{\boldsymbol{r}_1}\|^2/\sigma_n^2 \\ & - \sum_{k=1}^{K_c}\sum_{i=2}^{M} \|\boldsymbol{r}_i^k - \hat{\alpha}_{i,1}^{(c)}\boldsymbol{F}^H\boldsymbol{\Gamma}_{i,1}^k\boldsymbol{F}\bar{\boldsymbol{r}_k}\|^2/\sigma_n^2. \end{aligned} \tag{43}$$

Because $\bar{\boldsymbol{r}}_1$ and $\bar{\boldsymbol{r}}_k$ are unknown, their estimates in (18) are used instead in (43). Note that $\boldsymbol{r}_i$ and $\boldsymbol{r}_i^k$ are independent of $\boldsymbol{\theta}$, by negating the sign of (43), neglecting constants and after some straight forward mathematical calculations, a cost function equivalent to the one in (43) but to be minimized, is given by

$$\begin{aligned} Q_4(\boldsymbol{\theta}) = & -\left(1+\hat{\boldsymbol{\alpha}}^T\hat{\boldsymbol{\alpha}}\right)\bar{\boldsymbol{r}_1}^H\bar{\boldsymbol{r}_1} \\ & -\left(1+(\hat{\boldsymbol{\alpha}}^{(c)})^T\hat{\boldsymbol{\alpha}}^{(c)}\right)\sum_{k=1}^{K_c}\bar{\boldsymbol{r}_k}^H\bar{\boldsymbol{r}_k}, \end{aligned} \tag{44}$$

where the relative weighting factors are respectively $w_s = (1 + \hat{\boldsymbol{\alpha}}^T\hat{\boldsymbol{\alpha}})$ and $w_c = (1 + (\hat{\boldsymbol{\alpha}}^{(c)})^T\hat{\boldsymbol{\alpha}}^{(c)})$.

By using arbitrary positive weighting factors, the cost function in (44) can be modified as

$$Q_5(\boldsymbol{\theta}) = -w_s\bar{\boldsymbol{r}_1}^H\bar{\boldsymbol{r}_1} - w_c\sum_{k=1}^{K_c}\bar{\boldsymbol{r}_k}^H\bar{\boldsymbol{r}_k}, \tag{45}$$

where $w_s > 0$ and $w_c > 0$ denote respectively the weighting factors of source signal and reference signals. As mentioned in [31], the steepest descent direction of GN method for original cost function in (44) is given by

$$\boldsymbol{\Delta}_{\boldsymbol{\theta}} = -\left\{\frac{\partial^2 Q_4(\boldsymbol{\theta})}{\partial\boldsymbol{\theta}\partial\boldsymbol{\theta}^T}\right\}^{-1}\frac{\partial Q_4(\boldsymbol{\theta})}{\partial\boldsymbol{\theta}}. \tag{46}$$

And the Gauss-Newton descent direction of the modified cost function in (45) is given by

$$\tilde{\boldsymbol{\Delta}}_{\boldsymbol{\theta}} = -\left\{\frac{\partial^2 Q_5(\boldsymbol{\theta})}{\partial\boldsymbol{\theta}\partial\boldsymbol{\theta}^T}\right\}^{-1}\frac{\partial Q_5(\boldsymbol{\theta})}{\partial\boldsymbol{\theta}}. \tag{47}$$

Compared with $\boldsymbol{\Delta}_{\boldsymbol{\theta}}$, $\tilde{\boldsymbol{\Delta}}_{\boldsymbol{\theta}}$ is not the steepest descent direction for (44), but it is indeed a descent direction because

$$\begin{aligned} Q_5(\boldsymbol{\theta}+\tilde{\boldsymbol{\Delta}}_{\boldsymbol{\theta}}) &\approx Q_5(\boldsymbol{\theta}) - \frac{\partial Q_5(\boldsymbol{\theta})}{\partial\boldsymbol{\theta}}^T\left\{\frac{\partial^2 Q_5(\boldsymbol{\theta})}{\partial\boldsymbol{\theta}\partial\boldsymbol{\theta}^T}\right\}^{-1}\frac{\partial Q_5(\boldsymbol{\theta})}{\partial\boldsymbol{\theta}} \\ &\le Q_5(\boldsymbol{\theta}), \end{aligned} \tag{48}$$

which roots in the positive definite property of $\{\frac{\partial^2 Q_5(\boldsymbol{\theta})}{\partial\boldsymbol{\theta}\partial\boldsymbol{\theta}^T}\}$. Therefore, using the modified cost function in (45) instead of (44), we can eventually obtain the final solution which minimizes $Q_4(\boldsymbol{\theta})$, given a small enough tolerance as the stopping criteria. However, the cost may be that more iterations are needed before convergence is achieved.

APPENDIX B
EVALUATION OF JACOBIAN AND HESSIAN MATRICES

In this appendix, we give detailed formulations for evaluating the Jacobian matrix and Hessian matrix of $Q_2(\boldsymbol{\theta})$ in (28) with respect to $\boldsymbol{\theta} = [\boldsymbol{\delta}^T, \boldsymbol{u}^T]^T$.

For $Q_2(\boldsymbol{\theta})$ in (28), taking the first order partial derivative of it with respect to $\boldsymbol{\theta}$ yields

$$\begin{aligned} \boldsymbol{D}_1 = & \left(\sum_{i=2}^{M}\frac{\partial\boldsymbol{U}_{1,i}}{\partial d_i}\left(\frac{\partial d_i}{\partial\boldsymbol{\theta}}\right)^T\right)^H\sum_{i=1}^{M}\boldsymbol{U}_{1,i} \\ & + \sum_{k=1}^{K_c}\left(\sum_{i=2}^{M}\frac{\partial\boldsymbol{U}_{2,i}^k}{\partial d_i^k}\left(\frac{\partial d_i^k}{\partial\boldsymbol{\theta}}\right)^T\right)^H\sum_{i=1}^{M}\boldsymbol{U}_{2,i}^k, \end{aligned} \tag{49}$$

where

$$\begin{aligned} \frac{\partial\boldsymbol{U}_{1,i}}{\partial d_i} &= \boldsymbol{F}^H\tilde{\boldsymbol{n}}\boldsymbol{\Gamma}_{2,1}^H\boldsymbol{F}\boldsymbol{r}_i \\ \frac{\partial\boldsymbol{U}_{2,i}^k}{\partial d_i^k} &= \boldsymbol{F}^H\tilde{\boldsymbol{n}}(\boldsymbol{\Gamma}_{2,1}^k)^H\boldsymbol{F}\boldsymbol{r}_i^k, \end{aligned} \tag{50}$$

and $\frac{\partial d_i}{\partial\boldsymbol{\theta}} = [\boldsymbol{0}_{1\times(i-2)}, 1, \boldsymbol{0}_{1\times(M-i)}, \boldsymbol{\rho}_i^T - \boldsymbol{\rho}_1^T]^T$, $\frac{\partial d_i^k}{\partial\boldsymbol{\theta}} = [\boldsymbol{0}_{1\times(i-2)}, 1, \boldsymbol{0}_{1\times(M-i)}, \boldsymbol{0}_{1\times d}]^T$. Taking the partial derivative of $\boldsymbol{D}_1$ with respect to $\boldsymbol{\theta}^T$, the Hessian matrix $\boldsymbol{D}_2$ is given as

$$\begin{aligned} \boldsymbol{D}_2 = & \left(\sum_{i=2}^{M}\frac{\partial\boldsymbol{U}_{1,i}}{\partial d_i}\right)^H\left(\sum_{i=1}^{M}\boldsymbol{U}_{1,i}\right)\frac{\partial^2 d_i}{\partial\boldsymbol{\theta}\partial\boldsymbol{\theta}^T} \\ & + \left(\sum_{i=2}^{M}\frac{\partial^2\boldsymbol{U}_{1,i}}{\partial d_i^2}\right)^H\left(\sum_{i=1}^{M}\boldsymbol{U}_{1,i}\right)\frac{\partial d_i}{\partial\boldsymbol{\theta}}\left(\frac{\partial d_i}{\partial\boldsymbol{\theta}}\right)^T \\ & + \sum_{k=1}^{K_c}\left(\sum_{i=2}^{M}\frac{\partial^2\boldsymbol{U}_{2,i}^k}{\partial(d_i^k)^2}\right)^H\left(\sum_{i=1}^{M}\boldsymbol{U}_{2,i}^k\right)\frac{\partial d_i^k}{\partial\boldsymbol{\theta}}\left(\frac{\partial d_i^k}{\partial\boldsymbol{\theta}}\right)^T, \end{aligned} \tag{51}$$

where

$$\begin{aligned} \frac{\partial^2\boldsymbol{U}_{1,i}}{\partial d_i^2} &= \boldsymbol{F}^H(\tilde{\boldsymbol{n}})^2\boldsymbol{\Gamma}_{2,1}^H\boldsymbol{F}\boldsymbol{r}_i \\ \frac{\partial^2\boldsymbol{U}_{2,i}^k}{\partial(d_i^k)^2} &= \boldsymbol{F}^H(\tilde{\boldsymbol{n}})^2(\boldsymbol{\Gamma}_{2,1}^k)^H\boldsymbol{F}\boldsymbol{r}_i^k, \end{aligned} \tag{52}$$

and $\frac{\partial^2 d_i}{\partial\boldsymbol{\theta}\partial\boldsymbol{\theta}^T} = \text{blkdiag}(\boldsymbol{O}_{(M-1)\times(M-1)}, \boldsymbol{\rho}_2' - \boldsymbol{\rho}_1')$, with $\boldsymbol{\rho}_i' = (\boldsymbol{I}_d - \boldsymbol{\rho}_i\boldsymbol{\rho}_i^T)/\|\boldsymbol{u} - \boldsymbol{u}_i\|$.

ACKNOWLEDGMENT

The authors would like to thank the anonymous reviewers for their valuable comments that helped improve the quality of the paper.

REFERENCES

[1] D. J. Torrieri, "Statistical theory of passive location systems," *IEEE Trans. Aerosp. Electron. Syst.*, vol. AES-20, no. 2, pp. 183–198, Mar. 1984.

[2] S. Tomic, M. Beko, and R. Dinis, "RSS-based localization in wireless sensor networks using convex relaxation: Noncooperative and cooperative schemes," *IEEE Trans. Veh. Technol.*, vol. 64, no. 5, pp. 2037–2050, May 2015.

[3] Y. T. Chan and K. C. Ho, "A simple and efficient estimator for hyperbolic location," *IEEE Trans. Signal Process.*, vol. 42, no. 8, pp. 1905–1915, Aug. 1994.
[4] L. Yang and K. C. Ho, "An approximately efficient TDOA localization algorithm in closed-form for locating multiple disjoint sources with erroneous sensor positions," *IEEE Trans. Signal Process.*, vol. 57, no. 12, pp. 4598–4615, Dec. 2009.
[5] N. Patwari, A. O. Hero, M. Perkins, N. S. Correal, and R. J. O'Dea, "Relative location estimation in wireless sensor networks," *IEEE Trans. Signal Process.*, vol. 51, no. 8, pp. 2137–2148, Aug. 2003.
[6] Z. Wang and S. A. Zekavat, "A novel semidistributed localization via multinode TOA-DOA fusion," *IEEE Trans. Veh. Technol.*, vol. 58, no. 7, pp. 3426–3435, Sep. 2009.
[7] S. Al-Jazzar, J. Caffery, and H. You, "Scattering-model-based methods for TOA location in NLOS environments," *IEEE Trans. Veh. Technol.*, vol. 56, no. 2, pp. 583–593, Mar. 2007.
[8] X. Qu, L. Xie, and W. Tan, "Iterative constrained weighted least squares source localization using TDOA and FDOA measurements," *IEEE Trans. Signal Process.*, vol. 65, no. 15, pp. 3990–4003, Aug. 2017.
[9] H. Hmam, "Optimal sensor velocity configuration for TDOA-FDOA geolocation," *IEEE Trans. Signal Process.*, vol. 65, no. 3, pp. 628–637, Feb. 2017.
[10] J. O. Smith and J. S. Abel, "Closed-form least-squares source location estimation from range-difference measurements," *IEEE Trans. Acoust., Speech, Signal Process.*, vol. ASSP-35, no. 12, pp. 1661–1669, Dec. 1987.
[11] Y. Liu, F. Guo, L. Yang, and W. Jiang, "An improved algebraic solution for TDOA localization with sensor position errors," *IEEE Commun. Lett.*, vol. 19, no. 12, pp. 2218–2221, Dec. 2015.
[12] K. C. Ho, "Bias reduction for an explicit solution of source localization using TDOA," *IEEE Trans. Signal Process.*, vol. 60, no. 5, pp. 2101–2114, May 2012.
[13] A. Amar and A. J. Weiss, "Direct position determination (DPD) of multiple known and unknown radio-frequency signals," in *Proc. Eur. Signal Process. Conf.*, 2004, pp. 1115–1118.
[14] A. J. Weiss and A. Amar, "Direct geolocation of stationary wideband radio signal based on time delays and Doppler shifts," in *Proc. 2009 IEEE/SP 15th Workshop Statist. Signal Process.*, Aug. 2009, pp. 101–104.
[15] A. J. Weiss, "Direct geolocation of wideband emitters based on delay and Doppler," *IEEE Trans. Signal Process.*, vol. 59, no. 6, pp. 2513–2521, Jun. 2011.
[16] N. Vankayalapati, S. Kay, and Q. Ding, "TDOA based direct positioning maximum likelihood estimator and the Cramer-Rao bound," *IEEE Trans. Aerosp. Electron. Syst.*, vol. 50, no. 3, pp. 1616–1635, Jul. 2014.
[17] M. Pourhomayoun and M. L. Fowler, "Distributed computation for direct position determination emitter location," *IEEE Trans. Aerosp. Electron. Syst.*, vol. 50, no. 4, pp. 2878–2889, Oct. 2014.
[18] O. Bialer, D. Raphaeli, and A. J. Weiss, "Maximum-likelihood direct position estimation in dense multipath," *IEEE Trans. Veh. Technol.*, vol. 62, no. 5, pp. 2069–2079, Jun. 2013.
[19] J. Li, L. Yang, F. Guo, and W. Jiang, "Coherent summation of multiple short-time signals for direct positioning of a wideband source based on delay and Doppler," *Digit. Signal Process.*, vol. 48, pp. 58–70, Jan. 2016.
[20] E. Tzoreff and A. J. Weiss, "Expectation-maximization algorithm for direct position determination," *Signal Process.*, vol. 133, pp. 32–39, Apr. 2017.
[21] M. Rydstrom, E. G. Strom, and A. Svensson, "Clock-offset cancellation methods for positioning in asynchronous sensor networks," in *Proc. Int. Conf. Wireless Netw., Commun. Mobile Comput.*, Jun. 2005, pp. 981–986.
[22] Y. Wang and K. C. Ho, "TDOA source localization in the presence of synchronization clock bias and sensor position errors," *IEEE Trans. Signal Process.*, vol. 61, no. 18, pp. 4532–4544, Sep. 2013.
[23] C. Jia, J. Yin, W. Ding, and Z. Li, "Lagrange programming neural network for TOA-based localization with clock asynchronization and sensor location uncertainties," *Sensors*, vol. 7, pp. 3247–3263, 2019.
[24] B. Etzlinger, C. Pimminger, S. Fischereder, and A. Springer, "Passive localization and synchronization in the presence of affine clocks," in *Proc. Conf. Signals, Syst. Comput.*, 2016, pp. 1655–1658.
[25] O. Jean and A. J. Weiss, "Convex joint emitter localization and passive sensor network synchronization," in *Proc. Sensor Array Multichannel Signal Process. Workshop*, 2012, pp. 201–204.
[26] O. Jean and A. J. Weiss, "Passive localization and synchronization using arbitrary signals," *IEEE Trans. Signal Process.*, vol. 62, no. 8, pp. 2143–2150, Apr. 2014.
[27] X. Hui, Z. Chen, A. Wei, and B. Yang, "Robust TDOA localization algorithm for asynchronous wireless sensor networks," *Int. J. Distrib. Sensor Netw.*, vol. 2015, pp. 1–10, Jan. 2015.
[28] F. Ricciato, S. Sciancalepore, F. Gringoli, N. Facchi, and G. Boggia, "Position and velocity estimation of a non-cooperative source from asynchronous packet arrival time measurements," *IEEE Trans. Mobile Comput.*, vol. 17, no. 9, pp. 2166–2179, Sep. 2018.
[29] F. Ricciato, S. Sciancalepore, and G. Boggia, "Tracing a linearly moving node from asynchronous time-of-arrival measurements," *IEEE Commun. Lett.*, vol. 20, no. 9, pp. 1836–1839, Sep. 2016.
[30] F. Bandiera, A. Coluccia, G. Ricci, F. Ricciato, and D. Spano, "TDOA localization in asynchronous WSNs," in *Proc. IEEE Int. Conf. Embedded Ubiquitous Comput.*, 2014, pp. 193–196.
[31] S. Boyd and L. Vandenberghe, *Convex Optimization*. Cambridge, U.K.: Cambridge Univ. Press, 2004.
[32] M. Feder and E. Weinstein, "Parameter estimation of superimposed signals using the EM algorithm," *IEEE Trans. Acoust., Speech, Signal Process.*, vol. 36, no. 4, pp. 477–489, Apr. 1988.
[33] T. K. Moon, "The expectation-maximization algorithm," *IEEE Signal Process. Mag.*, vol. 13, no. 6, pp. 47–60, Nov. 1996.
[34] L. Lu, H. Wu, K. Yan, and S. S. Iyengar, "Robust expectation-maximization algorithm for multiple wideband acoustic source localization in the presence of nonuniform noise variances," *IEEE Sensors J.*, vol. 11, no. 3, pp. 536–544, Mar. 2011.
[35] A. Azevedo-Filho and R. D. Shachter, "Laplace's method approximations for probabilistic inference in belief networks with continuous variables," in *Uncertainty Proceedings*. San Mateo, CA, USA: Morgan Kaufmann, 1994, pp. 28–36.
[36] L. Davis, "Handbook of genetic algorithms, " in, *Handbook of Genetic Algorithms*. New York, NY, USA: Van Nostrand Reinhold, 1991.
[37] A. Y. Sidi and A. J. Weiss, "Delay and Doppler induced direct tracking by particle filter," *IEEE Trans. Aerosp. Electron. Syst.*, vol. 50, no. 1, pp. 559–572, Jan. 2014.
[38] S. M. Kay, *Fundamentals of Statistical Signal Processing: Estimation Theory*. Englewood Cliffs, NJ, USA: PTR Prentice-Hall, 1993.
[39] R. A. Horn and C. R. Johnson, *Matrix Analysis*. New York, NY, USA: Cambridge Univ. Press, 1986.
[40] A. Yeredor and E. Angel, "Joint TDOA and FDOA estimation: A conditional bound and its use for optimally weighted localization," *IEEE Trans. Signal Process.*, vol. 59, no. 4, pp. 1612–1623, Apr. 2011.

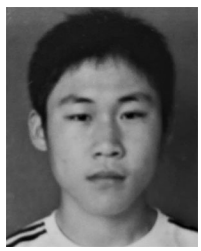

Fuhe Ma received the M.S. degree in statistical signal processing in 2016 from the National University of Defense Technology, Changsha, China, where he is currently working toward the Ph.D. degree. His research interests include passive localization and statistical signal processing.

Zhang-Meng Liu received the Ph.D degree in statistical signal processing from the National University of Defense Technology (NUDT), Changsha, China, in 2012. He is currently an Associate Professor with NUDT, working in the interdiscipline of electronics engineering and computer science, especially electronic data mining. From April 2017 to March 2018, he was a Visiting Scholar with the Big Data and Social Computing Laboratory, University of Illinois at Chicago, led by Prof. Philip S. Yu. He has authored or coauthored more than 30 journal papers on signal processing, Bayesian learning, and data mining.

Fucheng Guo received the B.S. and Ph.D. degrees from the National University of Defense Technology (NUDT), Changsha, China, in 1998 and 2002, respectively. From 2006 to 2007, he was a Visiting Scientist with the Xi'an Jiaotong University, Xi'an, China. From 2009 to 2010, he was a Visiting Scholar with the University of Missouri, Columbia, MO, USA. He is currently a Professor with the NUDT. His current research interests include passive localization, tracking, and radar/communication signal processing.